Human Molecular Genetics, 2011, Vol. 20, No. 14 **2710–2721**
doi:10.1093/hmg/ddr170
Advance Access published on April 19, 2011

Tissue-specific demethylation in CpG-poor promoters during cellular differentiation

Genta Nagae[1], Takayuki Isagawa[1], Nobuaki Shiraki[3], Takanori Fujita[1], Shogo Yamamoto[1], Shuichi Tsutsumi[1], Aya Nonaka[1], Sayaka Yoshiba[1], Keisuke Matsusaka[1,2], Yutaka Midorikawa[1], Shumpei Ishikawa[1,2], Hidenobu Soejima[4], Masashi Fukayama[2], Hirofumi Suemori[5], Norio Nakatsuji[6], Shoen Kume[3] and Hiroyuki Aburatani[1,*]

[1]Genome Science Division, Research Center for Advanced Science and Technology and [2]Department of Pathology, University of Tokyo, Tokyo, Japan, [3]Department of Stem Cell Biology, Institute of Molecular Embryology and Genetics, University of Kumamoto, Kumamoto, Japan, [4]Division of Molecular Genetics and Epigenetics, Department of Biomolecular Sciences, Faculty of Medicine, Saga University, Saga, Japan, [5]Laboratory of Embryonic Stem Cell Research, Stem Cell Research Center, Institute for Frontier Medical Sciences and [6]Institute for Integrated Cell-Material Sciences, Kyoto University, Kyoto, Japan

Received December 13, 2010; Revised and Accepted April 14, 2011

Epigenetic regulation is essential in determining cellular phenotypes during differentiation. Although tissue-specific DNA methylation has been studied, the significance of methylation variance for tissue phenotypes remains unresolved, especially for CpG-poor promoters. Here, we comprehensively studied methylation levels of 27 578 CpG sites among 21 human normal tissues from 12 anatomically different regions using an epigenotyping beadarray system. Remarkable changes in tissue-specific DNA methylation were observed within CpG-poor promoters but not CpG-rich promoters. Of note, tissue-specific hypomethylation is accompanied by an increase in gene expression, which gives rise to specialized cellular functions. The hypomethylated regions were significantly enriched with recognition motifs for transcription factors that regulate cell-type-specific differentiation. To investigate the dynamics of hypomethylation events, we analyzed methylation levels of the entire *APOA1* gene locus during *in vitro* differentiation of embryonic stem cells toward the hepatic lineage. A decrease in methylation was observed after day 13, coinciding with alpha-fetoprotein detection, in the vicinity of its transcription start sites (TSSs), and extends up to ~200 bp region encompassing the TSS at day 21, equivalent to the hepatoblastic stage. This decrease is even more pronounced in the adult liver, where the entire *APOA1* gene locus is hypomethylated. Furthermore, when we compared the methylation status of induced pluripotent stem (iPS) cells with their parental cell, IMR-90, we found that fibroblast-specific hypomethylation is restored to a fully methylated state in iPS cells after reprogramming. These results illuminate tissue-specific methylation dynamics in CpG-poor promoters and provide more comprehensive views on spatiotemporal gene regulation in terminal differentiation.

INTRODUCTION

In a series of differentiation processes during embryogenesis, a wide variety of cells are generated and organized in a spatiotemporal manner. They acquire distinctive patterns of gene expression to execute specialized cellular functions. In mammals, this gene specification is tightly regulated by multiple levels of epigenetic systems such as DNA methylation, histone modification, chromatin remodeling and noncoding RNA guidance (1,2). Mammalian cells coordinately regulate the complex transcriptional networks, which are essential for establishment of cellular programming and maintenance of given cellular phenotypes.

*To whom correspondence should be addressed at: Genome Science Division, Research Center for Advanced Science and Technology, 4-6-1 Komaba, Meguro-ku, Tokyo 153-8904, Japan. Tel: +81 354525352; Fax: +81 354525355; Email: haburata-tky@umin.ac.jp

DNA methylation has a strong impact on transcriptional repression. Because covalent modification of DNA itself is chemically stable when compared with other epigenetic marks, methylation-mediated repression is thought to be an effective mechanism to maintain long-lasting cell memories. Indeed, it plays pivotal roles in fundamental biological processes, including genome imprinting, retrotransposon silencing, X chromosome inactivation and tissue-specific gene expression (1). The lethality due to selective ablation of DNA methyltransferase with global loss of 5-methylcytosine also provides solid evidence for its significance in mammalian embryogenesis (3,4). Embryonic stem (ES) cells deficient in maintenance methyltransferase, *Dnmt1*, are viable, but die when induced to differentiate (5), demonstrating *Dnmt1* is essential for the dynamic epigenetic changes in cellular differentiation.

For many years, tissue-specific differentially methylated regions (tDMRs) have been of great interest (6–9). In somatic tissues, which include terminally differentiated cells, significant methylation variance between cells have been reported (6,8–11). Although recent technological advances in methylation profiling have broadened our understanding of the human methylome, we are still far from a comprehensive map required for deeper understanding of developmental epigenomics. That is partly because, due to technological limitations, most of earlier studies on human tDMRs have focused on CpG island promoters (12,13). In general, housekeeping genes, which constitutively express across many tissues, have such CpG-rich promoters. However, more than half the genes which have a tissue-specific pattern of expression have CpG-poor promoters (14). Therefore, it is important to analyze CpG-poor promoters in addition to CpG-rich promoters to elucidate regulatory changes of methylation during terminal differentiation.

Recent large-scaled methylation analyses of human normal tissues have revealed that methylation variance can be identified outside CpG islands and at CpG-poor promoters (6). The significance of methylation in the marginal regions of CpG islands (so-called CpG shore methylation) has been also proposed (15). In addition, tissue-specific binding of RNA polymerase II is often observed in CpG-poor promoters (16). These observations point to a significant role for epigenetic dynamics in CpG-poor promoters for terminal differentiation.

There are some difficulties in analyzing methylation levels in human tissue samples with accuracy. Cell populations in human tissues are not homogenous but rather are composed of a heterogeneous cell population which originates from different lineages. Because measurements of methylation are derived from these different methylomes of component cells, large differences in methylation between different cell types can be obscured. It is necessary to evaluate the methylation status quantitatively, rather than just qualitatively, to allow any comparison of methylation profiles between different samples. This requires good assay reproducibility to detect the more subtle methylation differences. In this study, we performed genome-wide promoter methylation analysis of human normal tissues using an epigenotyping beadarray system, which allows methylated CpG quantification in CpG-poor promoters as well as in CpG-rich promoters (17). We utilized inclusive probe sets for tissue-specific hypermethylation and hypomethylation, which occur mainly in CpG-poor promoters. Of note, we found that tissue-specific hypomethylation is well correlated with gene expression profiles that underlie tissue phenotypes. Around these cell-type-specific hypomethylated regions, binding motifs of particular transcription factors are remarkably enriched. These results suggest that a combination of tissue-specific promoter hypomethylation and selective binding of transcription factors is deeply involved in targeting specific genes during terminal differentiation. In addition, we demonstrated spreading of hypomethylation in CpG-poor promoters by *in vitro* cellular differentiation. The restoration of the fibroblast-specific hypomethylation was also observed during cellular reprogramming into induced pluripotent stem (iPS) cells. These results emphasize the importance of methylation dynamics in CpG-poor regions for multilayered epigenetic regulation in mammalian embryogenesis.

RESULTS

Genome-wide methylation analysis of human normal tissue reveals methylation variances in CpG-poor promoters

To develop a better understanding of methylation diversity among human normal tissues, we performed promoter methylation analysis of 21 human normal tissue samples from 12 anatomically different regions (Supplementary Material, Table S1). A HumanMethylation27 BeadChip® (Illumina, Inc) was used to quantify the methylation level of 27 578 CpG sites harboring 14 475 Refseq promoter regions (17).

First, we evaluated the accuracy and sensitivity of the assay using the modified DNA samples as methylation controls (0, 25, 50, 75 and 100% of methylation). The observed values of the methylated CpG ratio for the control samples were well correlated with the expected ratio of methylated CpGs (Supplementary Material, Fig. S1). Thus, methylation changes are quantitatively detectable using this system.

Next, we analyzed inter-individual methylation differences. The comparison plots of autosomal probes using biological duplicates of nine human tissues (brain, oral mucosa, lung, stomach, colon, liver, peripheral blood, kidney and skeletal muscle) showed good correlation between each pair (Pearson correlation coefficient; $r > 0.97$) (Supplementary Material, Fig. S2). For X-linked genes, most promoters on the inactivated allele are methylated in female cells. As expected, 0% methylation in male cells and ~50% methylation in female cells are accurately reported by the system (Supplementary Material, Fig. S2).

In this epigenotyping beadarray, most probes are designed to bind at and around the promoter regions, which are from 1.5 kb upstream to 1 kb downstream of transcription start sites (TSSs) of Refseq genes (Supplementary Material, Fig. S3). On the basis of the classification by the local CpG observed to expected ratio (CpG o/e) and the GC content ratio (GCR) around the probe, probes are divided into three groups: high-CpG density probes (HCG; CpG o/e > 0.75, GCR > 0.55), low-CpG density probes (LCG; CpG o/e < 0.48) and intermediate-CpG density probes (ICG; neither HCG nor LCG) (Supplementary Material, Fig. S4). The promoter methylation status is strongly affected by local CpG density. Most probes in relatively CpG-rich regions (HCG

and ICG) showed hypomethylation in all tissues, while more than half the probes in CpG-poor regions (LCG) are fully methylated (Supplementary Material, Fig. S5). To clarify the relationship between local CpG density and the methylation breadth among human normal tissues, we examined the tissue spatiality of hypermethylation (defined as methylation level more than 0.5) with regard to every autosomal probe ($n = 26\,486$). As shown in Figure 1, the methylation status of the LCG probes is highly variable among different tissues, whereas most CpG-rich probes are ubiquitously unmethylated. Therefore, the majority of intra-individual differences are observed in CpG-poor promoters.

Identification of tissue-specific hypermethylated and hypomethylated regions

To identify the tissue-specific differential gene methylation, we compared the methylation profiles of seven representative tissues. These were the brain and oral mucosa from the ectodermal lineage, the colon and liver from the endodermal lineage, the peripheral blood and skeletal muscle from the mesodermal lineage and the testis. First, we ranked the 26 486 autosomal probes in order of difference of the methylation level between the one tissue and the average of the other tissues. In case that tissue-specific hypomethylation or hypermethylation are sorted by the absolute values of the difference of the methylation level (more than 0.25 or less than -0.25), the number of distinctive gene sets varies widely (Supplementary Material, Fig. S6). There are more tissue-specific hypermethylated genes in the brain, liver, blood and testis than in other tissues. As for the hypomethylation, a large number of genes are selected in the testis and oral mucosa by this criterion. To evaluate the specific differential methylation equally among human tissues, we selected the top 250 probes of tissue-specific hypomethylation and hypermethylation for each tissue (Supplementary Material, Table S2). The methylation panel clearly shows specific hypomethylation as well as hypermethylation among seven tissues (Fig. 2A and B). We validated the methylation levels of the distinctive genes using the MassARRAY system. These methylation levels were consistent with the microarray data (Supplementary Material, Fig. S7). With respect to CpG density, most tissue-specific hypomethylated sites (80–90%) are associated with CpG-poor promoters (Fig. 2A and B). A notable exception was the testis, as testis-specific hypomethylated genes are associated with CpG-rich promoters. In CpG-rich promoter regions (HCP and ICP, $n = 18\,481$), ~900 regions ($5.10 \pm 0.48\%$) were found to be densely hypermethylated (mCpG > 70%) in somatic tissues. In the testis, only 286 regions (1.55%) were methylated (Supplementary Material, Fig. S5). These results are in agreement with earlier systematic screens that found the major fraction of tDMRs corresponding to CpG island methylation are either sperm- or testis-specific (6,9,10).

Variable hypomethylation patterns are associated with tissue-specific gene functions, gene expression patterns and selective binding of transcription factors

To characterize the gene function related to tissue-specific hypomethylation, we examined the enrichment of the specific

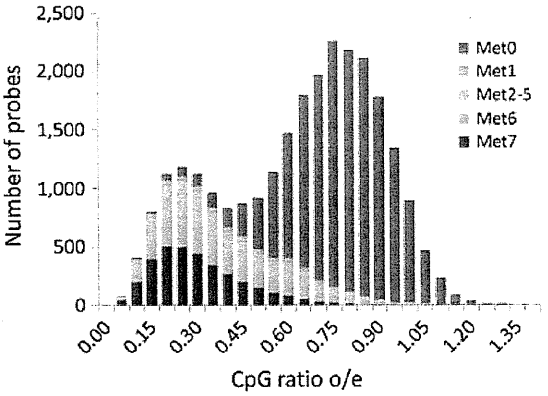

Figure 1. Methylation breadth among human normal tissues. The density histogram represents distribution of the CpG o/e around the probes with respect to the frequency of methylation among seven tissues. First, we generate the histogram of the numbers of probes with regard to CpG ratio o/e. Then, the methylation value of each probe is roughly divided into hypermethylation (0.0–1.0) or hypomethylation (0.0–0.5). Finally, each bar was partitioned by the number of tissues showing hypermethylation. For example, red bars (Met7) indicate all seven tissues are methylated, and blue bars (Met0) indicate no tissues are methylated.

gene ontology (GO) biological process categories in the top 250 hypomethylated gene sets. As shown in Table 1, the tissue-specific hypomethylated genes are closely related to cell-type-specific functions. For example, oral mucosa-specific hypomethylated genes show over-representation of genes related to ectoderm or epidermis development. In the gene set of liver-specific hypomethylation, we found several protein families synthesized by hepatocytes, such as serpin peptidase inhibitors and complement factors. Thus, these gene sets show over-representation of genes associated with acute inflammatory response. In the blood set, we found genes related to immune response, a key role for white blood cells. Genes related to the reproductive process are the major targets for CpG methylation in somatic cells besides sperm and its progenitor cells in the testis.

In contrast, we could not find any meaningful functional association between gene sets which undergo tissue-specific hypermethylation (Supplementary Material, Table S3). Although previous reports have identified a substantial number of confirmed sets of tissue-specific hypermethylation, it has been difficult to associate these with the tissue phenotype. *De novo* hypermethylation in differentiated cells might be often induced independently of functional specification.

While dense methylation of the CpG island promoter deeply contributes to gene silencing in pathological conditions such as cancer (18,19), the influence of sparse methylation in CpG-poor promoters on gene expression still remains controversial. CpG-poor promoters preferentially display the TATA box and numerous transcription factor-binding motifs around the TSS (20). Combinations of transcription factor binding in regulatory elements are involved in targeting gene expression. Thus, we analyzed expression levels of representative gene sets of tissue-specific hypomethylation and hypermethylation across seven human tissues (Fig. 3). The average expression level of hypomethylated genes is significantly higher than that of hypermethylated genes in a tissue-

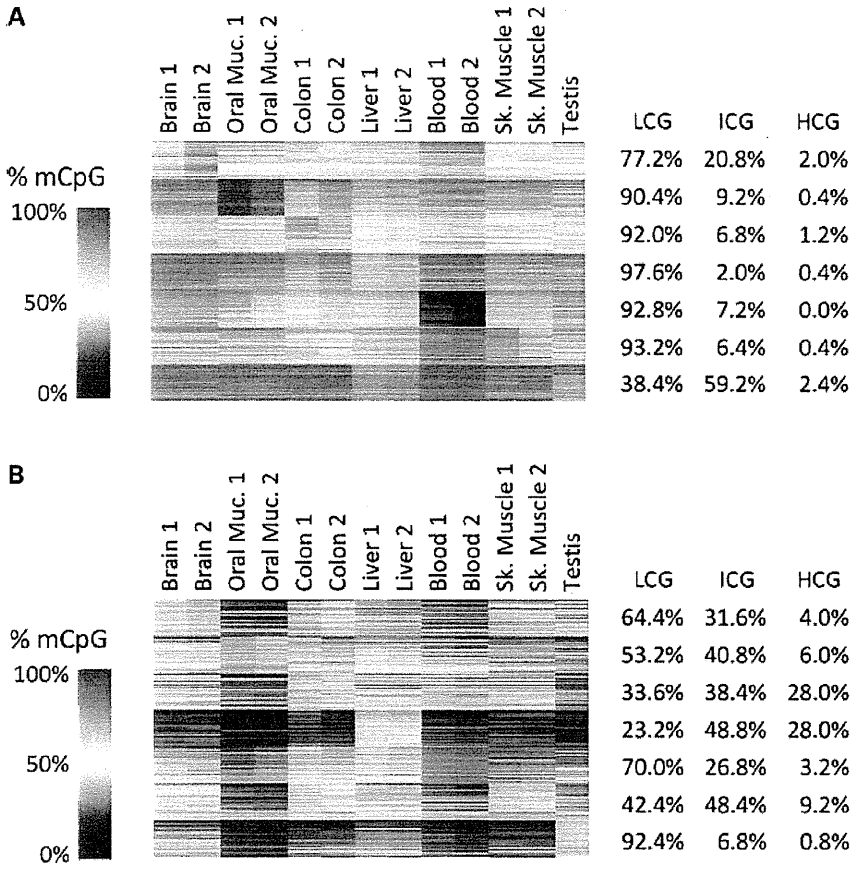

Figure 2. Methylation panel for tissue-specific differential methylation across seven human normal tissues. Left panels indicate the methylation levels of probe sets selected as tissue-specific hypomethylation (**A**) and as tissue-specific hypermethylation (**B**) among seven human tissues. Each row represents a CpG locus (250 for each tissue) and each column represents a tissue sample. The color scale bar at the left side shows the percentage of the methylation level (0–100%). The percentages of the LCG, ICG and HCG in a given probe set are represented at the right side.

specific manner. In contrast, tissue-specific hypermethylated genes are suppressed among all tissues. These results indicate that hypomethylation in the CpG-poor promoters identified here underlie tissue-specific expression in a given cell type.

Local epigenetic modification and recruitment of transcription factors are a fundamental part of the system for appropriate transcriptional regulation (21). We performed enrichment analysis of 746 recognition motifs for transcription factors to examine the relationship between cis-regulatory elements of promoters and tissue-specific hypomethylation. As shown in Figure 4, some matrices are significantly enriched (Z-score $>$ 8.0) in the hypomethylated regions. In oral-mucosa-specific hypomethylated regions, the binding motifs of p53 family genes are highly enriched. p63, the master regulator of keratinocyte differentiation, has similar DNA-binding domains to p53 and half of p63-bound regions in the squamous cell carcinoma cell line have p53 consensus motifs (22). In liver-specific hypomethylated regions, the matrices for the C4 zinc finger domain of the PPAR family (PPARA, PPARG and RXRs) and the NR2F family (HNF4A) are enriched compared with the background sequences. In the blood set, the matrices for the ETS domain of ETS factors (ETS1, ETS2, ELF2, ELK1) and the Runt domain of AML factors (RUNX1) are enriched. Similarly, MyoD-binding motifs are enriched in skeletal muscle-specific hypomethylated regions. In contrast, we could not find significant enrichment of transcription factor-binding motifs in tissue-specific hypermethylated regions (data not shown). Although the molecular mechanism of *de novo* hypermethylation and hypomethylation remains unknown, it is suggested that selective binding of transcription factors are at least significantly associated with regional hypomethylation during terminal differentiation.

Dynamic changes of CpG-poor promoter methylation during *in vitro* differentiation and cellular reprogramming

Although tissue-specific hypomethylation in CpG-poor promoters are closely related to gene specification for the tissue phenotype, when and how these variable methylation statuses are established remain unknown. To elucidate the methylation changes during cellular differentiation, we performed clustering analysis of human somatic tissue and normal cells

Table 1. GO analysis of tissue-specific hypomethylation

Tissue	GO term (biological process)	No. of genes	*P*-value
Brain	Nervous system development	28	4.22E − 05
	Multicellular organismal development	50	4.33E − 04
	Developmental process	53	4.64E − 04
Oral mucosa	Ectoderm development	20	4.89E − 14
	Epidermis development	18	2.19E − 12
	Tissue development	24	2.72E − 07
Colon	Defense response	31	3.68E − 11
	Response to stress	49	3.42E − 09
	Response to stimulus	71	7.31E − 07
Liver	Acute inflammatory response	20	9.00E − 19
	Response to wounding	34	7.22E − 16
	Response to external stimulus	43	3.72E − 15
Blood	Immune system process	55	6.86E − 24
	Immune response	42	2.53E − 19
	Defense response	33	2.62E − 13
Skeletal muscle	Muscle contraction	19	6.02E − 14
	Muscle system process	19	2.70E − 13
	Striated muscle contraction	9	2.64E − 08
Testis	Reproductive process in a multicellular organism	16	1.82E − 04
	Multicellular organism reproduction	16	1.82E − 04
	Gamete generation	14	2.40E − 04

including human ES cells, iPS cells and primary fibroblast cells using tissue-specific hypomethylation sites (Fig. 5). The heatmap shows distinct methylation patterns between the pluripotent cells and somatic tissues composed of the terminally differentiated cells. Seven human ES cell lines and two iPS cell lines show similar methylation patterns. Intriguingly, most genes representing specific hypomethylation in differentiated cells are densely methylated in both ES cells and iPS cells, raising the possibility that the default state of low CpG promoters in the embryonic stage is totally methylated and erasure of methylation may occur during terminal differentiation in a cell-type-specific manner.

We next compared the methylation status of the adult human liver and the fetal liver. Liver-specific hypomethylated genes are heavily methylated in KhES3, a human ES cell line, but are hypomethylated in the adult liver tissue (Fig. 6B and C). In the fetal liver, the methylation level of these genes shows a mild decrease in these regions. Bisulfite sequencing also revealed the partial hypomethylation of *ITIH3* and *APOA1* promoters (Supplementary Material, Fig S8A and B).

To further analyze the demethylation dynamics during hepatic differentiation, we analyzed methylation during *in vitro* differentiation toward hepatic lineages (23). On day 7, the cells began to express an endoderm marker, *SOX17* (Fig. 6A). *AFP* expression was detected on day 13 and *ALB* expression was detected on day 21. The methylation status of liver-specific hypomethylated genes showed a slight decrease during hepatic differentiation (Fig. 6B and C). Indeed, bisulfite sequencing of the *APOA1* promoter region demonstrated that CpG sites in this promoter region are fully hypermethylated in KhES3 and gradually become demethylated during *in vitro* differentiation (Supplementary Material, Fig. S8B). Demethylated regions are observed only in the vicinity of *APOA1* TSSs at day 21 of differentiation, and spread over 1 kb beyond the *APOA1* TSS in adult liver tissues. Sparse non-CpG methylation is observed in KhES3 and lost at day 21 of differentiation and also in adult liver tissues. This demethylation in non-CpG sites in KhES3 is also observed in the promoter region of *CD6* in adult blood and of *STMN4* in the adult brain (Supplementary Material, Fig. S9).

We then analyzed further the methylation status over the entire *APOA1* gene locus to determine the extent of demethylation events (Fig. 6D). Demethylation starts from the vicinity of *APOA1* TSSs at day 13 and extends to 200 bp around the TSS on day 21. Hypomethylated regions in human liver tissues spread over the *APOA1* region, from TSSs to the CpG island of the 3′ end and the further downstream region, suggesting the correlation of extensive demethylation with the stable expression of specific gene sets and cell fate determination.

Epigenetic reprogramming using defined factors enables terminally differentiated cells to gain pluripotency (24). Re-expression of pluripotency genes associated with these promoters, which are methylated in differentiated somatic cells, is important for iPS cell generation (25). The heatmap shows that the four human primary fibroblast cell lines (IMR90, MRC-9, KMS-6 and TIG-103) share specific hypomethylation. After cellular reprogramming into iPS cells, the IMR90 cells show restoration of methylation in these fibroblast-specific hypomethylated sites (Fig. 5). These results suggest that regaining promoter methylation in tissue-specific hypomethylated genes, as well as erasure of methylation in pluripotency genes, is important for this process.

DISCUSSION

In this study, we analyzed inclusive gene sets for tissue-specific hypomethylation and hypermethylation among human normal tissues. Of note, the former gene subsets are remarkably associated with cellular functions characterizing the tissue phenotypes. Although we have examined the limited sites of promoter regions, we reveal here that these hypomethylated genes display tissue-specific patterns of gene expression and specific enrichment of transcription factor recognition motifs in their promoters. This indicates the methylation changes in these regulatory regions might have functional roles in spatiotemporal transcriptional control. Furthermore, the hypomethylation panel showed an unexpected dense methylation pattern in pluripotent stem cells and regional hypomethylation in differentiated cells, suggesting this type of tDMRs might be a consequence of methylation erasure or a dilution process.

To date, the exploration of tDMRs was performed on the premise that stepwise addition of promoter methylation contributes to cell fate determination during early embryogenesis (26,27). It has been widely accepted that the genomic DNA of the embryo, which has pluripotency to differentiate into multiple lineages, is initially unmethylated and subsequent accumulations of hypermethylation in CpG island promoters are important for lineage restriction by reinforcing transcriptional repression of the unnecessary genes (28). Although

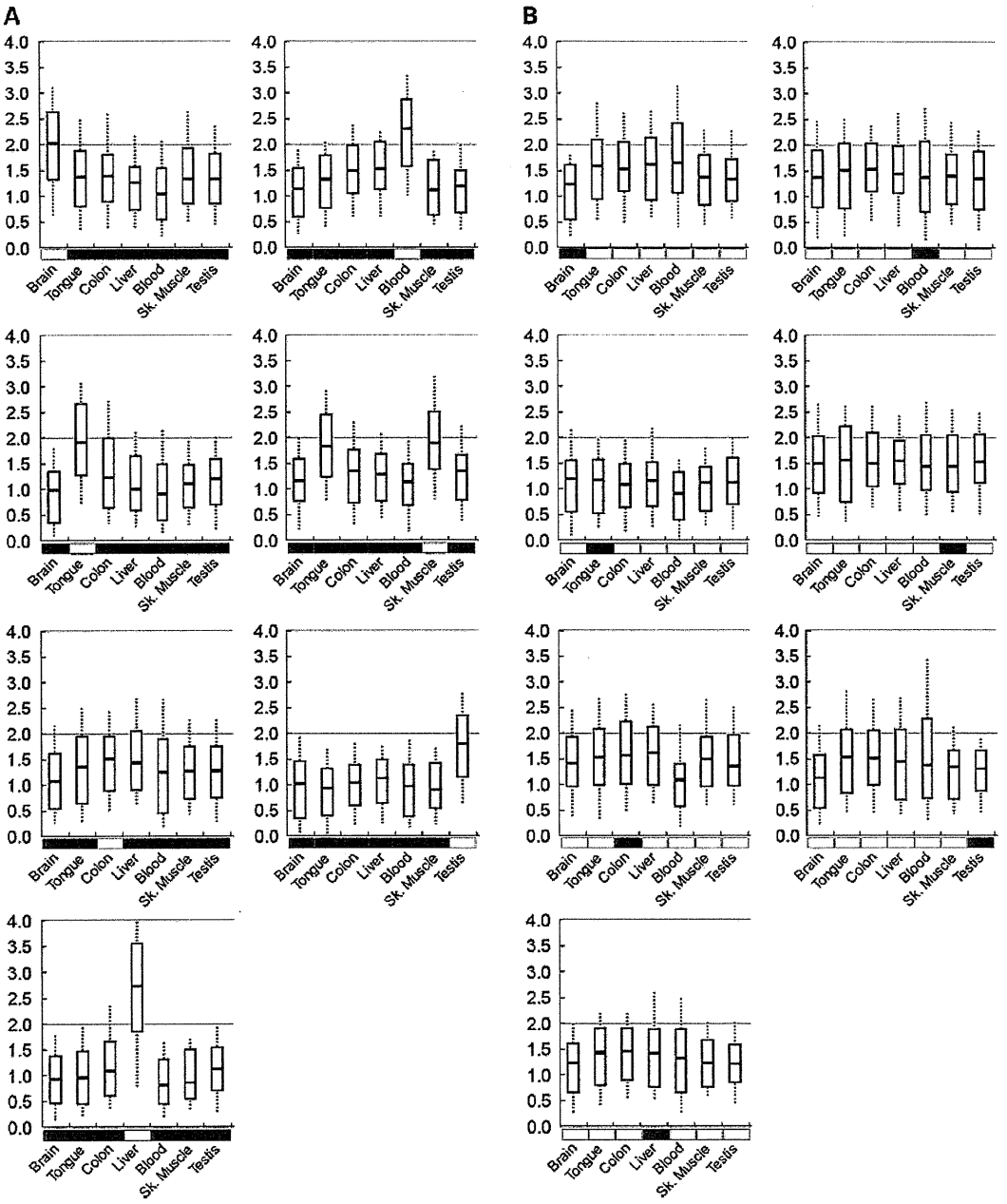

Figure 3. The gene expression level of tissue-specific differentially methylated genes. Shown box plots (from 25th percentile to the 75th percentile with heavy lines at the median) represent average gene expression levels (the log scale of the GeneChip score) of tissue-specific hypomethylated genes (**A**) and tissue-specific hypermethylated genes (**B**), for each tissue. The dotted lines extend above and below the box to show the first and ninth deciles. Black and white boxes below the bar graphs represent hypermethylation and hypomethylation of the given tissue, respectively.

this concept was true for some validated examples, it cannot adequately explain the global control of gene expression. In fact, consistent with the previous studies (6,10), we observed that most CpG island promoters are invariably unmethylated among normal tissues. In contrast with tissue-specific hypermethylation in CpG island promoters, tissue-specific hypomethylation in CpG-poor promoters has been underestimated so far and is significantly associated with the tissue phenotype.

These observations raise a new question about the molecular mechanism of tissue-specific hypomethylation established during terminal differentiation. Promoter demethylation in the differentiated cells is an old concept (29,30), but it has been forgotten while mammalian DNA demethylase was yet to be discovered. Now, two types of mechanisms for DNA demethylation, namely active demethylation and passive demethylation, are widely accepted for mammals (31,32).

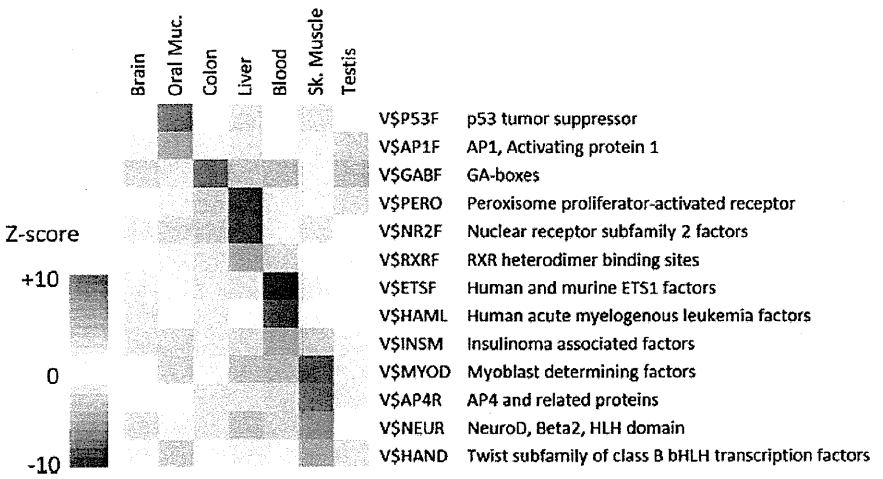

Figure 4. Enrichment of transcription factor recognition motifs in the tissue-specific hypomethylated regions. Each row represents a cis-regulatory module family with significant over-representation relative to a random set of mammalian promoters (Z-score > 8.0). Each column represents a tissue type. Four tissues (oral mucosa, liver, blood and skeletal muscle) show some specific enrichment of their master regulators binding motifs, respectively.

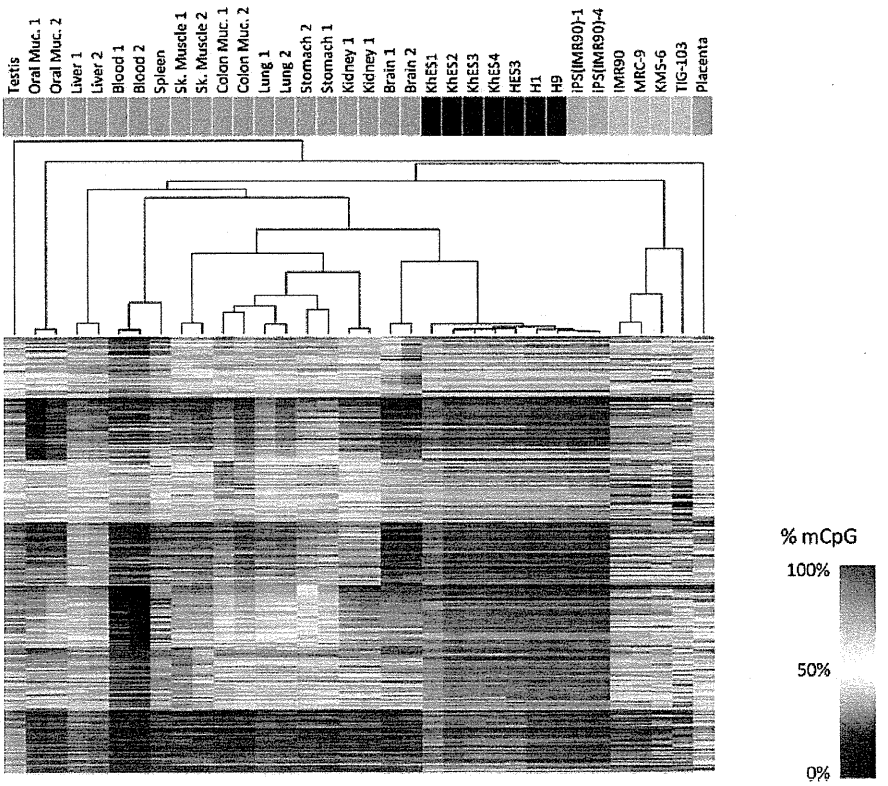

Figure 5. Hierarchical clustering analysis of human somatic tissues and normal cells. The dendrogram in the upper panel was obtained on the basis of the representative gene sets of tissue-specific hypomethylation using average linkage correlation. Each row represents a CpG locus (250 tissue-specific hypomethylation for each) and each column represents a sample. The colored boxes above the dendrogram indicate the nature of the samples; human somatic tissues (blue), human ES cells (red), human iPS cells (orange) and human primary fibroblast (green). The color scale bar at the right side shows the percentage of the methylation level (0–100%).

Active demethylation is observed in the paternal genome of an embryo during the first few days (33,34). In this process, demethylation occurs globally except for the limited foci such as imprinting control regions and centromeric and pericentromeric heterochromatin (35). Although recent reports suggested the ten-eleven translocation (TET) family proteins,

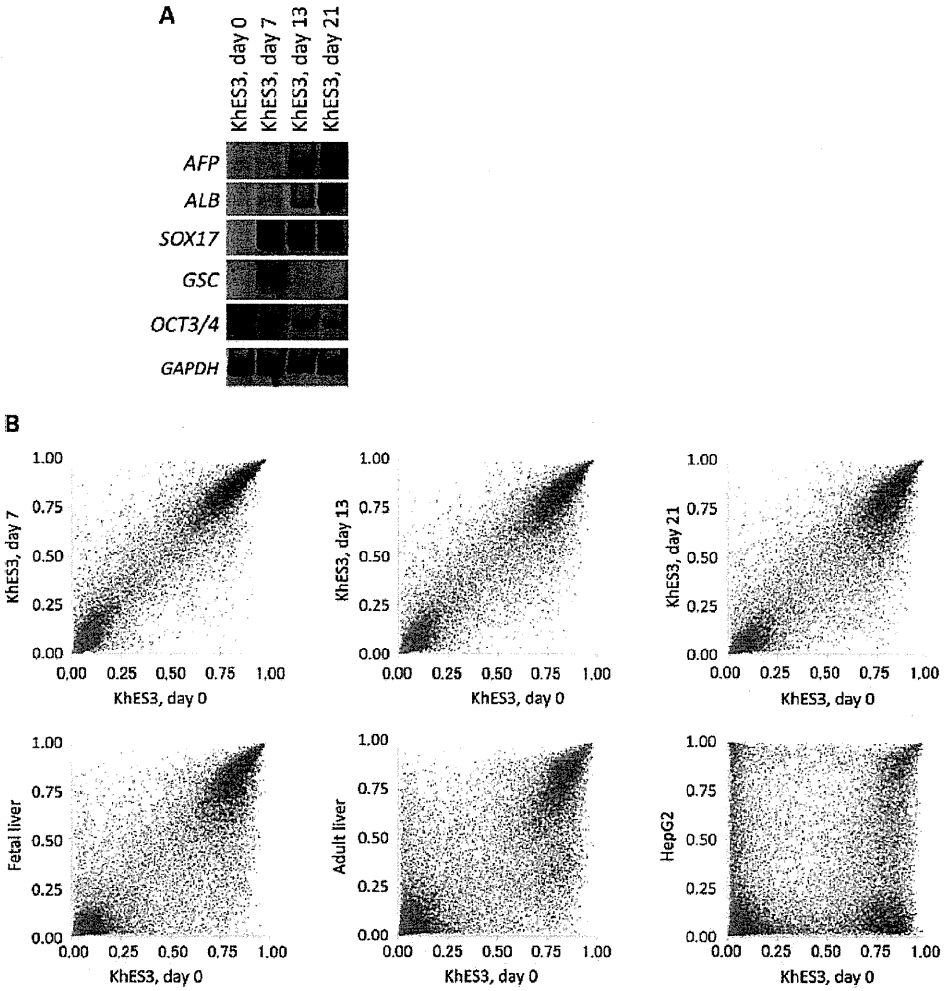

Figure 6. *In vitro* demethylation of liver-specific hypomethylated genes during hepatic differentiation (**A**) RT–PCR analysis of endodermal and hepatic differentiation markers in ES cells and differentiated cells (**B**) Global comparison among undifferentiated ES cells and differentiated cells, human fetal liver, adult liver and HepG2 cells. Liver-specific hypomethylated genes are indicated as red dots, overlapping with the others (blue). (**C**) Examples of gradually demethylated genes during *in vitro* differentiation into hepatic lineages. The bar graphs show the methylation levels of the genes that show gradual demethylation (~20% decrease) in day 21 of *in vitro* differentiation. (**D**) The liver-specific hypomethylated region around the *APOA1* gene. In the upper panel of the UCSC browser, nine black boxes indicate the position of PCR amplicons in a MassARRAY analysis. The methylation levels around the *APOA1* gene among ES cells and adult liver tissues are shown in the lower panel.

TET1, TET2 and TET3, are candidate proteins responsible for the erasure process through an oxidative demethylation pathway (32,36), further investigations are needed. The unexpected dynamics of DNA methylation during cellular differentiation might give us an important clue to elucidate the mechanism of cell fate determination during embryogenesis.

An alternative explanation for the tissue-specific demethylation seen in CpG-poor promoters is passive demethylation, which is usually observed in asymmetric cell division or highly proliferating cells like cancer cells. Inhibiting maintenance of cytosine methylation of the template strand could result in dilution of methylation in differentiated daughter cells. According to this scenario, transcription factor-related inhibition of DNA methyltransferase at the timing of cell division might be necessary because the developmental hypomethylation we observed here occurs not in a genome-wide manner but in a regional manner. Indeed, the enrichment of transcription factor-binding motifs is seen at the demethylated regions in a tissue-specific manner. Recently, it was shown that mitotically retained transcription factors are associated with the asymmetric cell division in some contexts (37,38). If sustained binding of transcription factors inhibits propagation of DNA methylation into the newly synthesized strand, transcription factor-driven demethylation will be inherited in proliferating cells. In our study, we examined *in vitro* differentiation in a series of promoters and found that a wave of demethylation develops from the TSS of *APOA1* and *ITIH3* promoters. Once the binding of transcription factors at demethylated regions induces gene expression in the tissue progenitor cells, sustained induction in response to appropriate extrinsic stimuli may result in loss of propagation of DNA methylation marks in the promoter regions for

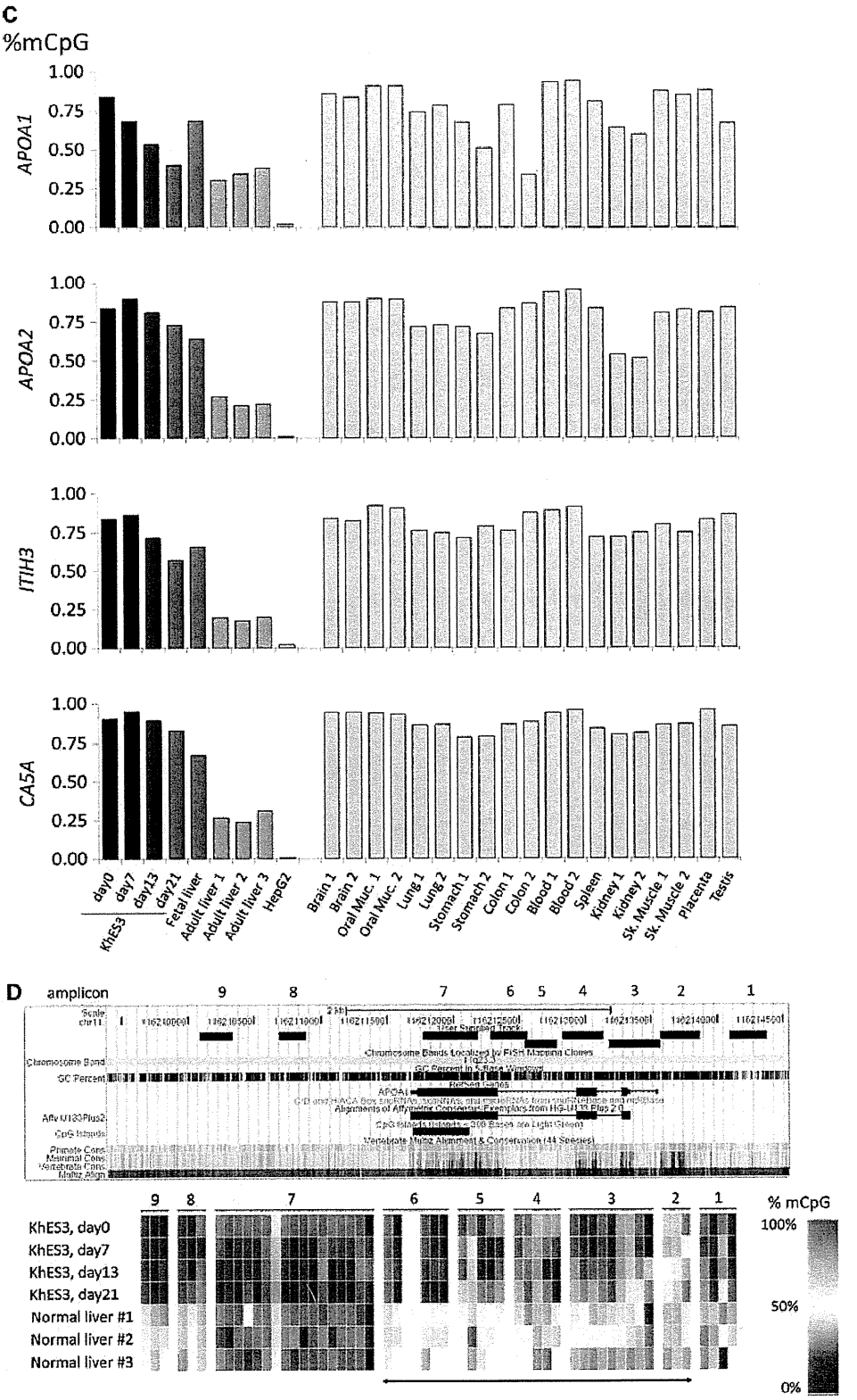

Figure 6. (Continued).

long-lasting maintenance of a transcriptionally active state. Subsequently, in this model, chromatin conformation changes in terminally differentiated cells would expand the demethylated regions and contribute to the establishment of stable and highly efficient expression of specific gene subsets.

Growing evidence suggests that forced induction of master regulator genes has the potential to change the fate of lineage-restricted cells, even in terminally differentiated cells (39–41). We identified restoration of methylation during reprogramming into iPS cells. The feasibility of cell reprogramming suggests that differentiated cells still have much more plasticity in the epigenetic status including DNA methylation than we had expected. Further analysis of methylation changes might provide novel insight into mechanisms that will generate a transcriptional repertoire for variable cell lineages and give us useful clues to control cell fate fixation, which might be applicable for regenerative medicine.

MATERIALS AND METHODS

Genomic DNA from human normal tissues

Frozen tissues of the brain, lung, liver and kidney were obtained from surgical specimens. Patients undergoing surgical resection at the Tokyo University General Hospital provided tissue after obtaining informed consent. Buccal swabs of oral mucosa, peripheral blood and placental tissue were from healthy volunteers. This study was certified by the Ethics Committee of Tokyo University. Genomic DNA from these clinical samples was extracted using the QIAamp DNA Mini Kit (QIAGEN). Genomic DNA of further individuals was purchased from BioChain (details are listed in Supplementary Material, Table S1). For the methylation-negative control, totally unmethylated genomic DNA was synthesized by a whole-genome amplification system, GenomiPhi (GE healthcare). For a positive control, fully methylated genomic DNA was generated by *Sss*.I CpG methylase (New England Biolabs) treatment of lymphocyte DNA.

Human ES cell lines

Human ES cell lines, KhES1, KhES2, KhES3, KhES4, were established and maintained as described previously (42). Human ES cell lines (H1, H9) and human iPS cell lines [iPS(IMR90)-1 and iPS(IMR90)-4] were obtained from WiCell Research Institute. HES3 cell line was obtained from ES Cell International.

Briefly, undifferentiated human ES cells were maintained on a feeder layer of MEF in DMEM/F12 (Sigma) supplemented with 20% KSR, l-Glu, NEAA and β-ME under 3% CO_2. To passage ES cells, ES cell colonies were detached from the feeder layer by treatment with 0.25% trypsin and 0.1 mg/ml of collagenase IV in PBS containing 20% KSR and 1 mm of $CaCl_2$ at 37°C for 5 min, followed by the addition of culture medium. ES cell clumps were disaggregated into smaller pieces by gentle pipetting.

An *in vitro* differentiation experiment was performed following the reported method, with some modification (43). Briefly, KhES3 cells were cultured in differentiation medium [RPMI supplemented with human recombinant activin A (100 ng/ml) and defined FBS]. FBS concentrations were 0% for the first 24 h, 0.2% for the second 48 h and 2.0% for subsequent days of differentiation. Media were replaced every 2 days with fresh differentiation medium supplemented with growth factors. ES cells were cultured in differentiation medium (DMEM supplemented with 10% KSR, Dex and HGF) for up to 30 days.

Methylation profiling

Methylation status was analyzed using HumanMethylation27 BeadChip (Illumina). Genomic DNA for methylation profiling was quantified using the Quant-iT dsDNA BR Assay Kit (Invitrogen). Five hundred nanograms of genomic DNA was bisulfite-converted using an EZ DNA Methylation Kit (Zymo Research). The converted DNA was amplified, fragmented and hybridized to a BeadChip according to the manufacturer's instructions. The raw signal intensity for both methylated (M) and unmethylated (U) DNA was measured using a BeadArray Scanner (Illumina). The methylation level of the each individual CpG is obtained using the formula (M)/(M)+(U)+100 by the GenomeStudio (Illumina).

Quantitative methylation analysis using the MassARRAY system

Bisulfite treatment of genomic DNA was performed using an EZ Methylation Kit (Zymo Research). Primer sequences are given in Supplementary Material, Table S4. This system utilizes MALDI-TOF mass spectrometry in combination with RNA base-specific cleavage (MassCLEAVE). A detectable pattern is analyzed for the methylation status. Mass spectra were acquired using a MassARRAY Compact MADLI-TOF (Sequenom) and spectra's methylation ratios were generated using Epityper software v1.0 (Sequenom).

Bisulfite sequencing

Bisulfite sequencing analysis was performed as described previously (44). Bisulfite treatment of genomic DNA was performed using an EZ Methylation Kit (Zymo Research). All primer sequences and melting temperatures for the polymerase chain reaction (PCR) are given in Supplementary Material, Table S4. PCR amplicons were subcloned into the pGEM-T vector (Promega). Clones were sequenced using PRISM3100 Sequencer (Applied Biosystems).

RNA extraction and gene expression microarray analysis

Genome-wide analysis of mRNA expression levels using U133plus2.0 human expression array® (Affymetrix) was done essentially as described previously (45). Briefly, total RNA was isolated using TRIzol reagent (Invitrogen), according to the manufacturer's instructions. One microgram of RNA was used for the generation of double-stranded cDNA with the SuperScript Double-Stranded cDNA Synthesis Kit (Invitrogen) according to the manufacturer's protocol. Double-stranded cDNAs were hybridized to the microarray.

Reverse transcription–polymerase chain reaction analysis

RNA extraction and reverse transcription–polymerase chain reaction (RT–PCR) were done as described (46). Total RNA was extracted using TRI Reagent (Sigma-Aldrich) or the RNeasy micro-kit (Qiagen) and then treated with DNase (Sigma-Aldrich). Three micrograms of RNA was reverse-transcribed using Moloney Murine Leukemia Virus reverse transcriptase (Toyobo, Japan) and oligo(dT) primers (Toyobo). The primer sequences are shown in Supplementary Material, Table S4. The PCR conditions for each cycle were as follows: denaturation at 96°C for 30 s, annealing at 60°C for 2 s and extension at 72°C for 45 s. RT–PCR products were separated by 5% non-denaturing polyacrylamide gel electrophoresis, stained with SYBR Green I (Molecular Probes), and visualized using a Gel Logic 200 Imaging System (Kodak).

Definition of probe classes and promoter classes

We classified 27 578 probes into three categories: HCG, ICG and LCG. Each probe position was defined with respect to the position of a given CpG site. We determined the GC content and the ratio of observed versus expected CpG dinucleotides in a surrounding 500 bp window. The CpG ratio was calculated using the following formula: (number of CpGs × number of bp) (number of Cs × number of Gs). Three categories of probes were determined as follows: (i) HCGs (8098 probes) covering a 500 bp area with a CpG ratio above 0.75 and GC content above 55%; (ii) LCGs (8374 probes) excluded from a 500 bp area with a CpG ratio above 0.48; and (iii) ICGs (11 106 probes) that could not be categorized as either HCGs or LCGs.

Clustering analysis

To analyze the similarity of the methylation levels among human somatic tissues, ES cells and iPS cells, we used the data set of tissue-specific hypomethylation selected in Figure 2A for the cluster analysis. We applied a hierarchical clustering algorithm using the uncentered correlation coefficient as the measure of similarity and average linkage clustering (47) and visualized the dendrogram and the heatmap using TreeView (48).

GO functional annotation analysis

GO functional annotations for differentially hypomethylated and hypermethylated gene sets were performed using the Database for Annotation, Visualization and Integrated Discovery (DAVID) Bioinformatic Resources v6.7 (http://niaid.abcc.ncifcrf.gov/ home.jsp). The lists of 250 gene symbols that show specific hypermethylation or hypermethylation for each tissue were submitted and DAVID default population background (*Homo sapiens*) was chosen to detect significantly over-represented GO biological processes (GOTERM BP-FAT). *P*-values were calculated by a modified Fisher's exact test and adjusted for multiple hypotheses testing using Bonferroni correction. The three GO terms with the most significant *P*-value and the number of genes involved in the term were listed for each tissue.

Enrichment analysis of transcription factor-binding motifs

To determine over-represented transcription factor-binding sites in tissue-specific hypomethylated and hypermethylated regions, sequences around the probe within a 500 bp window were screened for the presence of binding sites using Genomatix RegionMiner (http://www.genomatix.de, matrix library version 7.1). The number of binding site motifs was determined and over-representation over the background of random mammalian promoter sequences was calculated as the *Z*-score. Transcription factor families with a Z-score greater than 8.0 were considered highly significant. The *Z*-scores of these representative TF modules are visualized in the heatmap using TreeView (48).

SUPPLEMENTARY MATERIAL

Supplementary Material is available at *HMG* online.

ACKNOWLEDGEMENTS

We are grateful to Hiroko Meguro for microarray experiment, Kaoru Nakano for MassARRAY analysis, Elodie Lebredonchel for bisulfite sequencing experiment and Michael Jones for critical reading of the manuscript.

Conflict of Interest statement. None declared.

FUNDING

This work was mainly supported by a Grant-in-Aid for Scientific Research (S) 20221009 (H.A.) from the Ministry of Education, Culture, Sports, Science and Technology (MEXT), Japan, and the Program of Fundamental Studies in Health Sciences of the National Institute of Biomedical Innovation (NIBIO), Japan.

REFERENCES

1. Bird, A. (2002) DNA methylation patterns and epigenetic memory. *Genes Dev.*, **16**, 6–21.
2. Bernstein, B.E., Meissner, A. and Lander, E.S. (2007) The mammalian epigenome. *Cell*, **128**, 669–681.
3. Li, E., Bestor, T.H. and Jaenisch, R. (1992) Targeted mutation of the DNA methyltransferase gene results in embryonic lethality. *Cell*, **69**, 915–926.
4. Okano, M., Bell, D.W., Haber, D.A. and Li, E. (1999) DNA methyltransferases Dnmt3a and Dnmt3b are essential for de novo methylation and mammalian development. *Cell*, **99**, 247–257.
5. Jackson-Grusby, L., Beard, C., Possemato, R., Tudor, M., Fambrough, D., Csankovszki, G., Dausman, J., Lee, P., Wilson, C., Lander, E. *et al.* (2001) Loss of genomic methylation causes p53-dependent apoptosis and epigenetic deregulation. *Nat. Genet.*, **27**, 31–39.
6. Rakyan, V.K., Down, T.A., Thorne, N.P., Flicek, P., Kulesha, E., Graf, S., Tomazou, E.M., Backdahl, L., Johnson, N., Herberth, M. *et al.* (2008) An integrated resource for genome-wide identification and analysis of human tissue-specific differentially methylated regions (tDMRs). *Genome Res.*, **18**, 1518–1529.
7. Khulan, B., Thompson, R.F., Ye, K., Fazzari, M.J., Suzuki, M., Stasiek, E., Figueroa, M.E., Glass, J.L., Chen, Q., Montagna, C. *et al.* (2006)

Comparative isoschizomer profiling of cytosine methylation: the HELP assay. *Genome Res.*, **16**, 1046–1055.
8. Shen, L., Kondo, Y., Guo, Y., Zhang, J., Zhang, L., Ahmed, S., Shu, J., Chen, X., Waterland, R.A. and Issa, J.P. (2007) Genome-wide profiling of DNA methylation reveals a class of normally methylated CpG island promoters. *PLoS Genet.*, **3**, 2023–2036.
9. Straussman, R., Nejman, D., Roberts, D., Steinfeld, I., Blum, B., Benvenisty, N., Simon, I., Yakhini, Z. and Cedar, H. (2009) Developmental programming of CpG island methylation profiles in the human genome. *Nat. Struct. Mol. Biol.*, **16**, 564–571.
10. Eckhardt, F., Lewin, J., Cortese, R., Rakyan, V.K., Attwood, J., Burger, M., Burton, J., Cox, T.V., Davies, R., Down, T.A. *et al.* (2006) DNA methylation profiling of human chromosomes 6, 20 and 22. *Nat. Genet.*, **38**, 1378–1385.
11. Illingworth, R., Kerr, A., DeSousa, D., Jorgensen, H., Ellis, P., Stalker, J., Jackson, D., Clee, C., Plumb, R., Rogers, J. *et al.* (2008) A novel CpG island set identifies tissue-specific methylation at developmental gene loci. *PLoS Biol.*, **6**, e22.
12. Laird, P.W. (2010) Principles and challenges of genome-wide DNA methylation analysis. *Nat. Rev. Genet.*, **11**, 191–203.
13. Waterland, R.A., Kellermayer, R., Rached, M.T., Tatevian, N., Gomes, M.V., Zhang, J., Zhang, L., Chakravarty, A., Zhu, W., Laritsky, E. *et al.* (2009) Epigenomic profiling indicates a role for DNA methylation in early postnatal liver development. *Hum. Mol. Genet.*, **18**, 3026–3038.
14. Saxonov, S., Berg, P. and Brutlag, D.L. (2006) A genome-wide analysis of CpG dinucleotides in the human genome distinguishes two distinct classes of promoters. *Proc. Natl Acad. Sci. USA*, **103**, 1412–1417.
15. Irizarry, R.A., Ladd-Acosta, C., Carvalho, B., Wu, H., Brandenburg, S.A., Jeddeloh, J.A., Wen, B. and Feinberg, A.P. (2008) Comprehensive high-throughput arrays for relative methylation (CHARM). *Genome Res.*, **18**, 780–790.
16. Barrera, L.O., Li, Z., Smith, A.D., Arden, K.C., Cavenee, W.K., Zhang, M.Q., Green, R.D. and Ren, B. (2008) Genome-wide mapping and analysis of active promoters in mouse embryonic stem cells and adult organs. *Genome Res.*, **18**, 46–59.
17. Bibikova, M., Le, J., Barnes, B., Saedinia-Melnyk, S., Zhou, L., Shen, R. and Gunderson, K.L. (2009) Genome-wide DNA methylation profiling using infinium assay. *Epigenomics*, **1**, 177–200.
18. Jones, P.A. and Takai, D. (2001) The role of DNA methylation in mammalian epigenetics. *Science*, **293**, 1068–1070.
19. Walsh, C.P. and Bestor, T.H. (1999) Cytosine methylation and mammalian development. *Genes Dev.*, **13**, 26–34.
20. Baek, D., Davis, C., Ewing, B., Gordon, D. and Green, P. (2007) Characterization and predictive discovery of evolutionarily conserved mammalian alternative promoters. *Genome Res.*, **17**, 145–155.
21. Kadonaga, J.T. (1998) Eukaryotic transcription: an interlaced network of transcription factors and chromatin-modifying machines. *Cell*, **92**, 307–313.
22. Yang, A., Zhu, Z., Kapranov, P., McKeon, F., Church, G.M., Gingeras, T.R. and Struhl, K. (2006) Relationships between p63 binding, DNA sequence, transcription activity, and biological function in human cells. *Mol. Cell*, **24**, 593–602.
23. Shiraki, N., Umeda, K., Sakashita, N., Takeya, M., Kume, K. and Kume, S. (2008) Differentiation of mouse and human embryonic stem cells into hepatic lineages. *Genes Cells*, **13**, 731–746.
24. Takahashi, K. and Yamanaka, S. (2006) Induction of pluripotent stem cells from mouse embryonic and adult fibroblast cultures by defined factors. *Cell*, **126**, 663–676.
25. Wernig, M., Meissner, A., Foreman, R., Brambrink, T., Ku, M., Hochedlinger, K., Bernstein, B.E. and Jaenisch, R. (2007) *In vitro* reprogramming of fibroblasts into a pluripotent ES-cell-like state. *Nature*, **448**, 318–324.
26. Cedar, H. and Bergman, Y. (2009) Linking DNA methylation and histone modification: patterns and paradigms. *Nat. Rev. Genet.*, **10**, 295–304.
27. Weber, M., Hellmann, I., Stadler, M.B., Ramos, L., Paabo, S., Rebhan, M. and Schubeler, D. (2007) Distribution, silencing potential and evolutionary impact of promoter DNA methylation in the human genome. *Nat. Genet.*, **39**, 457–466.
28. Reik, W. (2007) Stability and flexibility of epigenetic gene regulation in mammalian development. *Nature*, **447**, 425–432.
29. Bergman, Y. and Mostoslavsky, R. (1998) DNA demethylation: Turning genes on. *Biol. Chem.*, **379**, 401–407.
30. Eden, S. and Cedar, H. (1994) Role of DNA methylation in the regulation of transcription. *Curr. Opin. Genet. Dev.*, **4**, 255–259.
31. Ooi, S.K.T. and Bestor, T.H. (2008) The colorful history of active DNA demethylation. *Cell*, **133**, 1145–1148.
32. Wu, S.C. and Zhang, Y. (2010) Active DNA demethylation: many roads lead to Rome. *Nat. Rev. Mol. Cell Biol.*, **11**, 607–620.
33. Mayer, W., Niveleau, A., Walter, J., Fundele, R. and Haaf, T. (2000) Embryogenesis: demethylation of the zygotic paternal genome. *Nature*, **403**, 501–502.
34. Oswald, J., Engemann, S., Lane, N., Mayer, W., Olek, A., Fundele, R., Dean, W., Reik, W. and Walter, J. (2000) Active demethylation of the paternal genome in the mouse zygote. *Curr. Biol.*, **10**, 475–478.
35. Reik, W., Dean, W. and Walter, J. (2001) Epigenetic reprogramming in mammalian development. *Science*, **293**, 1089–1093.
36. Ito, S., D'Alessio, A.C., Taranova, O.V., Hong, K., Sowers, L.C. and Zhang, Y. (2010) Role of Tet proteins in 5mC to 5hmC conversion, ES-cell self-renewal and inner cell mass specification. *Nature*, **466**, 1129–1133.
37. Young, D.W., Hassan, M.Q., Yang, X.-Q., Galindo, M., Javed, A., Zaidi, S.K., Furcinitti, P., Lapointe, D., Montecino, M., Lian, J.B. *et al.* (2007) Mitotic retention of gene expression patterns by the cell fate-determining transcription factor Runx2. *Proc. Natl Acad. Sci. USA*, **104**, 3189–3194.
38. Zaidi, S.K., Young, D.W., Montecino, M.A., Lian, J.B., van Wijnen, A.J., Stein, J.L. and Stein, G.S. (2010) Mitotic bookmarking of genes: a novel dimension to epigenetic control. *Nat. Rev. Genet.*, **11**, 583–589.
39. Takahashi, K., Tanabe, K., Ohnuki, M., Narita, M., Ichisaka, T., Tomoda, K. and Yamanaka, S. (2007) Induction of pluripotent stem cells from adult human fibroblasts by defined factors. *Cell*, **131**, 861–872.
40. Vierbuchen, T., Ostermeier, A., Pang, Z.P., Kokubu, Y., Sudhof, T.C. and Wernig, M. (2010) Direct conversion of fibroblasts to functional neurons by defined factors. *Nature*, **463**, 1035–1041.
41. Ieda, M., Fu, J.-D., Delgado-Olguin, P., Vedantham, V., Hayashi, Y., Bruneau, B.G. and Srivastava, D. (2010) Direct reprogramming of fibroblasts into functional cardiomyocytes by defined factors. *Cell*, **142**, 375–386.
42. Suemori, H., Yasuchika, K., Hasegawa, K., Fujioka, T., Tsuneyoshi, N. and Nakatsuji, N. (2006) Efficient establishment of human embryonic stem cell lines and long-term maintenance with stable karyotype by enzymatic bulk passage. *Biochem. Biophys. Res. Commun.*, **345**, 926–932.
43. D'Amour, K.A., Agulnick, A.D., Eliazer, S., Kelly, O.G., Kroon, E. and Baetge, E.E. (2005) Efficient differentiation of human embryonic stem cells to definitive endoderm. *Nat. Biotech.*, **23**, 1534–1541.
44. Hayashi, H., Nagae, G., Tsutsumi, S., Kaneshiro, K., Kozaki, T., Kaneda, A., Sugisaki, H. and Aburatani, H. (2007) High-resolution mapping of DNA methylation in human genome using oligonucleotide tiling array. *Hum. Genet.*, **120**, 701–711.
45. Hippo, Y., Watanabe, K., Watanabe, A., Midorikawa, Y., Yamamoto, S., Ihara, S., Tokita, S., Iwanari, H., Ito, Y., Nakano, K. *et al.* (2004) Identification of soluble NH2-terminal fragment of glypican-3 as a serological marker for early-stage hepatocellular carcinoma. *Cancer Res.*, **64**, 2418–2423.
46. Shiraki, N., Yoshida, T., Araki, K., Umezawa, A., Higuchi, Y., Goto, H., Kume, K. and Kume, S. (2008) Guided differentiation of embryonic stem cells into Pdx1-expressing regional-specific definitive endoderm. *Stem Cells*, **26**, 874–885.
47. Eisen, M.B., Spellman, P.T., Brown, P.O. and Botstein, D. (1998) Cluster analysis and display of genome-wide expression patterns. *Proc. Natl Acad. Sci. USA*, **95**, 14863–14868.
48. Saldanha, A.J. (2004) Java Treeview–extensible visualization of microarray data. *Bioinformatics*, **20**, 3246–3248.

Am J Physiol Heart Circ Physiol 301: H1723–H1741, 2011.
First published August 19, 2011; doi:10.1152/ajpheart.00553.2011.

Review

Pathophysiology of myocardial reperfusion injury: preconditioning, postconditioning, and translational aspects of protective measures

Shoji Sanada,[1] Issei Komuro,[1] and Masafumi Kitakaze[2]

[1]Department of Cardiovascular Medicine, Osaka University Graduate School of Medicine, and [2]Department of Cardiovascular Medicine, National Cerebral and Cardiovascular Center, Suita, Japan

Submitted 31 May 2011; accepted in final form 15 August 2011

Sanada S, Komuro I, Kitakaze M. Pathophysiology of myocardial reperfusion injury: preconditioning, postconditioning, and translational aspects of protective measures. *Am J Physiol Heart Circ Physiol* 301: H1723–H1741, 2011. First published August 19, 2011; doi:10.1152/ajpheart.00553.2011.—Heart diseases due to myocardial ischemia, such as myocardial infarction or ischemic heart failure, are major causes of death in developed countries, and their number is unfortunately still growing. Preliminary exploration into the pathophysiology of ischemia-reperfusion injury, together with the accumulation of clinical evidence, led to the discovery of ischemic preconditioning, which has been the main hypothesis for over three decades for how ischemia-reperfusion injury can be attenuated. The subcellular pathophysiological mechanism of ischemia-reperfusion injury and preconditioning-induced cardioprotection is not well understood, but extensive research into components, including autacoids, ion channels, receptors, subcellular signaling cascades, and mitochondrial modulators, as well as strategies for modulating these components, has made evolutional progress. Owing to the accumulation of both basic and clinical evidence, the idea of ischemic postconditioning with a cardioprotective potential has been discovered and established, making it possible to apply this knowledge in the clinical setting after ischemia-reperfusion insult. Another a great outcome has been the launch of translational studies that apply basic findings for manipulating ischemia-reperfusion injury into practical clinical treatments against ischemic heart diseases. In this review, we discuss the current findings regarding the fundamental pathophysiological mechanisms of ischemia-reperfusion injury, the associated protective mechanisms of ischemic pre- and postconditioning, and the potential seeds for molecular, pharmacological, or mechanical treatments against ischemia-reperfusion injury, as well as subsequent adverse outcomes by modulation of subcellular signaling mechanisms (especially mitochondrial function). We also review emerging translational clinical trials and the subsistent clinical comorbidities that need to be overcome to make these trials applicable in clinical medicine.

calcium overload; reactive oxygen species; mitochondria; transition pore; comorbidities; clinical trials

WHAT DO WE KNOW ABOUT ischemia-reperfusion injury? Because the morbidity and mortality due to ischemic heart diseases have come to the fore in developed countries and are still increasing, it is critically important, both scientifically and socially, to know how cardioprotection is achieved in ischemic myocardium. In fact, in the clinical setting, the application of coronary thrombolysis or immediate percutaneous coronary intervention for faster recanalization has been shown to dramatically improve the outcomes of patients with acute or chronic myocardial ischemia due to impaired coronary blood supply. This finding is founded on the premise that a shorter period of index ischemia causes less damage (212).

However, even if the ischemic period is short or limited, the functional recovery of a reperfused heart is often less successful than expected due to "reperfusion injury" (188), and we still do not have a definitive intervention to eliminate reperfusion-induced myocardial damage. Therefore, it is important to fully understand the mechanisms of ischemia-reperfusion injuries and to consider cardioprotective strategies.

Dynamic Sequence of Ischemia-Reperfusion Injury

ATP depletion as the original hypothesis. To maintain cellular homeostasis, the intracellular use of both ATP and high-energy phosphates is critically important. Cellular energy metabolism depends on acetyl-CoA, which is generated through aerobic/anaerobic glycolysis or β-oxidation of free fatty acids and is then metabolized through the tricarboxylic acid cycle, which supplies ATP. Cardiomyocytes are rich in mitochondria because the highest continuous amount of ATP is consumed within the myocardium, and this demand for ATP can only be met by aerobic metabolism. When hearts are exposed to ischemia, coronary arterioles and resistant vessels significantly

Address for reprint requests and other correspondence: M. Kitakaze, Dept. of Cardiovascular Medicine, National Cerebral and Cardiovascular Ctr., 5-7-1, Fujishirodai, Suita, 565-8565, Japan (e-mail: kitakaze@zf6.so-net.ne.jp).

dilate to increase coronary blood flow up to three to five times above basal levels and to supply as much oxygen as possible and maintain aerobic needs. However, because of the lack of anaerobic metabolic pathways, the absence of a supply of oxygen leads to the depletion of intramyocardial ATP in a short period of time, making the myocardium very susceptible to ischemia.

Initial studies on ischemic myocardium revealed that contractile arrest generally occurs within several minutes of index ischemia, followed by cellular bulging and rupture of intracellular microstructures starting 15 to 30 min later (4). This discovery led to the ATP depletion hypothesis as a central cause of cell death because a 90% decrease in ATP results in irreversible structural changes in the myocardium (4). Therefore, supplementation of ATP in the myocardium was initially proposed as an effective therapy for the prevention of ischemic myocardial death.

However, a complete depletion of ATP within the myocardium takes ~40–60 min, whereas the intracellular inorganic phosphate level promptly increases just after the onset of ischemia (120), suggesting the rapid exhaustion of intracellular high-energy phosphate. Therefore, it was then thought that a change in the intracellular pH was a trigger for this lethal cascade.

Decreasing pH and counterbalancing Ca^{2+} accumulation. Anaerobic glycolysis prevails in ischemic myocardium, causing a rapid decrease in the intracellular pH and deactivation of troponin C sensitivity to phosphofructokinase and Ca^{2+}. Within several minutes, this decrease results in contractile arrest and cellular bulging. To buffer this decrease in pH, excessive H^+ is excreted by accelerated Na^+/H^+ exchange, which in turn causes substantial Na^+ inflow (152). Meanwhile, intracellular ATP depletion gradually inactivates ATPases, such as the Na^+/K^+ ATPase, ATP-dependent Ca^{2+} reuptake, and active Ca^{2+} excretion, resulting in Ca^{2+} overload. These results have also been confirmed in vivo (121). These changes are also accompanied by a subsequent activation of intracellular proteases, such as calpain, which causes a fragile cellular structure, hypercontracture, which leads to contraction band necrosis, and the initiation of apoptotic cascades (Fig. 1) and mitochondrial transition pore opening, which will be discussed later. Each of these factors can occur within minutes, but they proceed gradually because a low intracellular pH slows or inhibits all of them (76). This idea agrees with the observation that reoxygenation within 5 min avoids irreversible cellular damage, whereas index ischemia for more than 15 min gradually affects intracellular structures (123).

Rapid normalization of pH and overload of Ca^{2+} and reactive oxygen species upon reperfusion. Prompt reperfusion or reoxygenation will bring about a rapid restoration of substrates essential for the generation of ATP, such as glucose or free fatty acids, an instantaneous increase in the oxygen supply, and prompt normalization of the extracellular pH by pericellular washout. Indeed, all of these factors are crucial for the prevention of further ischemic cellular injury and for restoration of cellular homeostasis; however, they can also concurrently cause reperfusion injury (188). Rapid normalization of the extracellular pH will instantly create an extreme H^+ gradient across the plasma membrane that triggers a robust Na^+/H^+ exchange and a massive Na^+ influx. This unphysiological gradient can instantly trigger the passive, inverted action of the surface Na^+/Ca^{2+} exchanger, called "reverse mode," which absorbs Na^+ accumulation via excretion but, in turn, allows intracellular Ca^{2+} overload (179) (Fig. 2). Meanwhile, rapid normalization of intracellular pH disinhibits a low pH-derived inhibition of the Ca^{2+}-dependent protease calpain, hypercontracture, and the mitochondrial permeability transition all at once and promptly accelerates myocardial damage in the early stages of reperfusion (76). This also occurs when, upon reoxygenation, ectopic xanthine oxidase is activated by Ca^{2+}-sensitive proteases (89) and the intramitochondrial respiratory chain. This activation causes a sudden recovery of aerobic metabolism and results in an overload of reactive oxygen species (ROS), mainly superoxide. Physiologically, superoxide becomes hydrogen peroxide via superoxide dismutase (SOD) (53), which is then inactivated by catalase and becomes H_2O and O_2. However, robust ROS generation beyond this catalytic process generates excessive hydroxyl radicals, which are very unstable but have a high potential to damage cellular structures, enzymes, or channel proteins on the cellular membrane (200). These events, together with activation of inflammatory cascades and facilitation of bioactive autacoids, such as cytokines or catecholamines, make cells more susceptible to death (Fig. 3) or myocardial contractile

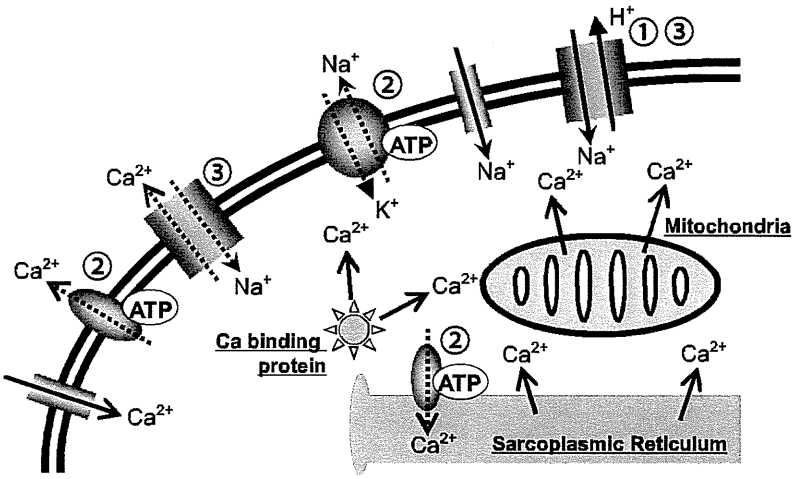

Fig. 1. Ion exchanges during ischemia: *1*) excretion of H^+ due to pH lowering, *2*) deactivation due to loss of ATP, and *3*) reduction of Na^+/Ca^{2+} exchange due to lowered extracellular pH and intracellular accumulation of Na^+.

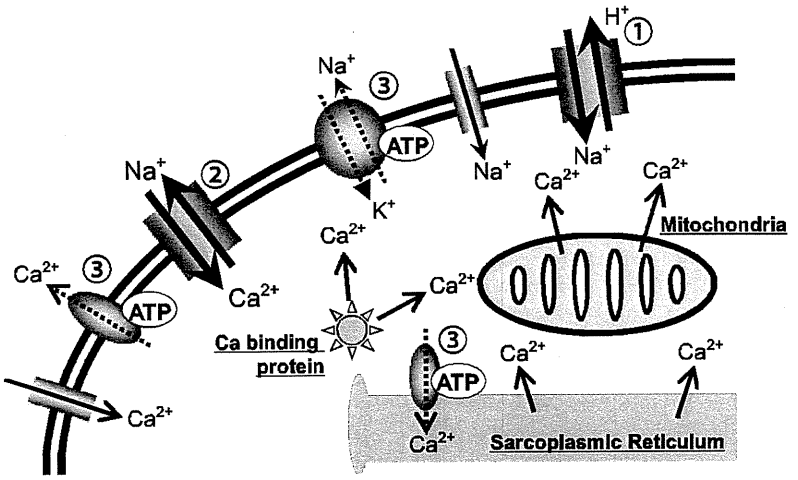

Fig. 2. Ion exchanges at reperfusion: *1*) robust excretion of H^+ due to prompt recovery of extracellular pH, *2*) "reverse mode" excretion of accumulated Na^+ and Ca^{2+} influx in turn, and *3*) reexcretion of Ca^{2+} followed by recovery of ATP synthesis.

dysfunction (183) immediately after the onset of reperfusion. Furthermore, impaired intracellular Ca^{2+} and ROS regulation can propagate to adjacent cells through gap junctions to further spread injury (159). Finally, after 30–60 min of reperfusion, a gradual recovery of Ca^{2+} excretion and ATP-dependent Ca^{2+} reuptake in sarcoplasmic reticulum takes place, and the cells return to homeostasis. This ischemia-reperfusion process makes the intracellular Ca^{2+} concentration dual peaked (120), with one peak occurring at 15–60 min after the onset of index ischemia and the other peak occurring within 30 min of reperfusion.

Various modes of death and their regulation under ischemia-reperfusion. During the above sequence of events, Ca^{2+} overload and excessive ROS generation can trigger multiple modes of cell death, such as necrosis and apoptosis (168). Myocardial necrotic changes generally include cellular swelling as an initial change, followed by rupture of cellular membranes, degradation of intracellular proteins or structures induced by Ca^{2+}-dependent proteases such as calpain (89), Ca^{2+}-induced hypercontracture [which induces mechanical rupture of muscle fibers (159)], and direct cleavage of DNA by free radicals originating from excessive ROS. Necrotic changes often require focal recruitment of inflammatory cells for subsequent scavenging activity.

Apoptosis is usually triggered by intracellular Ca^{2+} overload, which induces the processing of procaspase-8 into active caspase-8 and the activation of Bax, which lead to the release of the apoptosis-inducing factor, Smac, and cytochrome-*c* from mitochondria. Apoptosis-inducing factor translocates into the nucleus and facilitates nonspecific DNA fragmentation. Smac inactivates X chromosome-linked inhibitor of apoptosis protein, which inhibits caspase-3, and cytochrome-*c* forms an apoptosome complex with procaspase-9 and apoptotic protease-activating factor-1, which activates caspase-9. Together, these cascades ultimately contribute to irreversible cellular dysfunction. Ca^{2+} accumulation (57) and ROS induction (175) are also crucial for opening the pore that enables trafficking of nonspecific, small molecules across mitochondrial membranes. Subsequently, H^+ influx into mitochondria and a decrease in the mitochondrial membrane potential result in mitochondrial

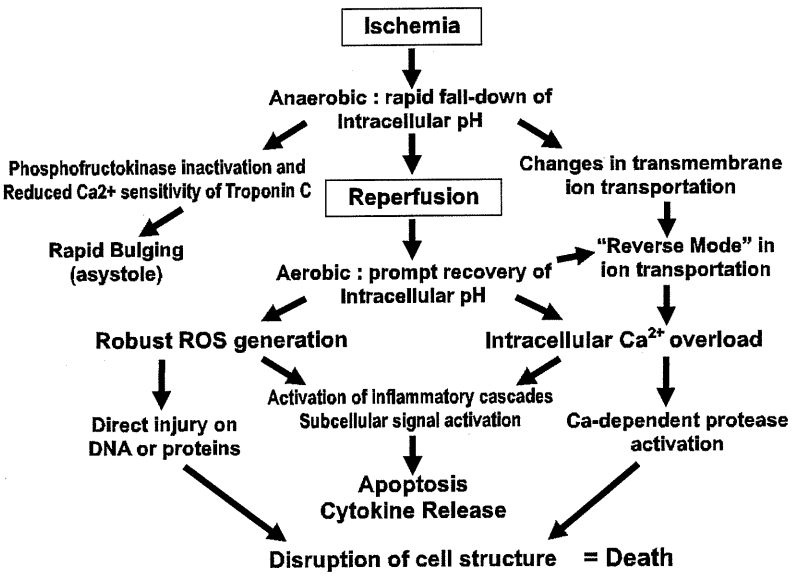

Fig. 3. Putative cascades of cell death due to ischemia-reperfusion injury. ROS, reactive ocygen species.

swelling and apoptotic changes (66). Histological findings of apoptosis include nuclear chromatin condensation, making cells nonfunctional, followed by cellular shrinking and fragmentation, usually independently of the inflammatory reaction, and subsequent phagocytotic clearance (7).

Necrosis prevails within the ischemic myocardium and its adjacent regions, whereas apoptosis predominantly occurs in the ischemic border and in nonischemic regions (202), reflecting the differences in the focal magnitude of anoxia, ROS accumulation, neurohormonal activation, and mechanical stress. Recent reports propose that necrotic cell death prevails when the intramitochondrial Ca^{2+} level becomes extremely low or completely lost (14). Similarly, the intracellular ATP level might also serve as a "molecular switch," with high levels resulting in apoptosis and low levels resulting in necrosis (105).

Adaptation and therapeutic targets for ischemia-reperfusion injury. Because the prompt recovery of intracellular pH and reoxygenation enhances Ca^{2+} overload or ROS generation and promotes reperfusion injury as described above in *Rapid normalization of pH and overload of Ca^{2+} and reactive oxygen species upon reperfusion* and *Various modes of death and their regulation under ischemia-reperfusion*, it has long been proposed that the transient acidosis during early reperfusion (97) as well as acidic or staged reperfusion procedures (67) buffer the Ca^{2+} or ROS overload upon reperfusion. They can lead to a smaller infarct size or preservation of myocardial function (96, 97) by inhibiting Na^+/Ca^{2+} exchange and Ca^{2+} overload (91) or by directly disrupting proapoptotic signals (229), all of which might be important therapeutic targets of cardioprotection. Accordingly, some of the membrane ion channels, such as the Na^+/H^+ exchanger (228), the Na^+/K^+ ATPase (59), and the Ca^{2+}-activated K^+ channel (185), are possible candidates for cardioprotection due to preconditioning because of their ability to directly inhibit intracellular Ca^{2+} accumulation.

Another key therapeutic target might be excessive ROS production or prolonged catecholamine release. When myocardial ischemia occurs, presynaptic vesicles release norepinephrine via the accumulation of Na^+ and subsequent activation of reverse uptake-1 (180), which facilitates norepinephrine release. Norepinephrine activates both α-adrenoceptors that cause vasoconstriction and β-adrenoceptors that increase myocardial oxygen consumption. Both of these may make the cells more susceptive to ischemic damage. Indeed, many reports show that the blockade of the β-adrenoceptor will protect the myocardium from prolonged ischemia-reperfusion. However, possible pharmacological mechanisms other than hemodynamic benefits are under discussion (9, 180, 238).

On the other hand, there are a number of adaptive responses to the various kinds of stresses induced by ischemia-reperfusion, i.e., Ca^{2+} overload, ROS accumulation, neurohormonal stimuli, focal mechanical strain, and endoplasmic reticulum stress from excessive production of unfolded or misfolded proteins. Autophagy, the lysosomal bulk digestion pathway of intracellular structural proteins, contributes to physiological turnover as well as pathological removal of intracellular proteins as a housekeeping system. The process of autophagy begins by recruiting Atg-5, -12, and -16 to the intracellular lipid bilayer. These proteins are then polymerized by LC-3 to form the autophagosome. The autophagosome sequesters proteins targeted for destruction and then fuses with the protease-rich lysosome, resulting in digestion of its contents. Mitochondria also have an adaptive system involving dynamic fusion and "fission" with each other (222). A shift toward fusion favors the generation of interconnected mitochondria that form large networks and are beneficial in metabolically active cells against the dissipation of energy. Alternatively, a shift toward fission produces numerous mitochondrial fragments as morphologically and functionally distinct small spheres or short rods with an increased distribution and surface area, which is usually beneficial in quiescent cells (222). Therefore, the facilitation of autophagy (69) and mitochondrial fusion (141) might also protect against ischemia-reperfusion injury by maintaining intracellular homeostasis. In addition, the blockade of cell-to-cell connections, such as gap junctions, by modulating connexin-43 (136) could also protect the myocardium by blocking the propagation of cellular damage to neighboring cells (159) or by modulating mitochondrial ATP-sensitive K^+ (K_{ATP}) channel opening (164).

Discovery of Preconditioning

Before the concept of ischemic preconditioning arose, cardiologists observed that patients with severe, unstable angina or acute myocardial infarction and who had experienced at least one episode of prodromal angina often exhibited less chest pain, less variation in the ST segment of ECGs, less cardiac dysfunction, or even smaller myocardial infarct size. This was despite a paradoxical increase in the total period of time suffered from ischemia, and they called this the "cardiac warm-up phenomenon" (80). In 1986, Murry et al. (134) confirmed "preconditioning with ischemia" using an in vivo canine model and defined it as a phenomenon where brief periods of ischemia accompanied by reperfusion just before sustained ischemia exert *1*) a delay in ATP depletion, *2*) a reduction in oxygen consumption, *3*) a retention of intracellular structure, and *4*) a delay or reduction of cellular necrosis due to ATP expiration, finally resulting in delayed progression or reduction of infarct size, despite an increase in the total ischemic period. This is now recognized as a narrow definition of ischemic preconditioning. The concept of cardioprotection due to preconditioning currently prevails and has been expanded on to include not only acute irreversible injuries, such as necrosis and apoptosis, but also chronic disorders, such as myocardial hibernation or remodeling, although it appears to be irrelevant to acute myocardial contractile dysfunction, such as stunning (98).

Critical Dual Time Window: Early and Late Phases

The original report on preconditioning (134) also mentioned that the strength of protection by ischemic preconditioning critically depends on the duration from the end of preconditioning ischemia to the onset of index ischemia. Later, the existence of dual periods for this duration was reported (123). The first period is more than several seconds and <3 h and the second one, associated with the increased expression of cardioprotective heat shock proteins (HSPs) (123), is 24–72 h. These are now widely recognized as "early and late phase" preconditioning. The two phases appear to involve different types of reactions; the former involves reactions that are completed in a short period of time, such as activation of ion channels, phosphorylation/activation of existing enzymes, or

rapid turnover/translocation of substances, whereas the latter involves more time-consuming reactions, such as genomic modulation and expression of channel proteins, receptor proteins, enzymes, molecular chaperon proteins, or immunotransmitters.

Although these two phases differ in timing, they share some common triggers, mediators, and effectors. Finally, myocardial injury at the time of reperfusion might be a major target of both types of preconditioning as well as postconditioning; this will be discussed later (64).

Factors Underlying the Mechanisms of Preconditioning

G protein-coupled receptor agonists: adenosine, α- and β-adrenoceptor activation, and others. Downey and colleagues (109) opened the door to the investigation on mechanisms of preconditioning with a report showing that protection by ischemic preconditioning was abolished by the inhibition of the adenosine receptor before sustained ischemia in vivo. This suggested that adenosine was a trigger of ischemic preconditioning. However, they later reported a conflicting result in vitro that preischemic treatment with either adenosine or selective adenosine-A_1 receptor agonist, 2-chloro-N^6-cyclopentyladenosine, exerted minimal protection (49), implying that adenosine is not a candidate for pharmacological preconditioning. This inconsistency was highlighted by later reports from other groups showing successful pharmacological preconditioning with selective adenosine-A_1 receptor agonists, 2-chloro-N^6-cyclopentyladenosine or R-phenylisopropyladenosine, in early phase (130, 233) and late phase (91) infarct limitations in vivo, strongly suggesting the inclusion of adenosine receptor activation in ischemic preconditioning.

Later reports proposed α (68, 214)- and β (193, 209)-adrenoceptor activation as a putative trigger of ischemic preconditioning, based on the findings that receptor blockade abrogated ischemic preconditioning-induced cardioprotection. However, there were contradictory findings. Downey and colleagues reported that neither specific catecholamine receptor antagonists (207) nor depletion of intramyocardial catecholamine storage and release (8) blocked ischemic preconditioning, whereas exogenous catecholamine or adrenoceptor agonists did precondition the heart (207, 214). Vatner and colleagues also reported a similar observation that cardiac denervation did not block early phase but did blunt late-phase ischemic preconditioning via α_1-adrenoceptor signaling (102). In search of effective receptor subtypes, Tsuchida et al. showed the direct involvement of α_{1b}-adrenoceptor in ischemic preconditioning (214), but studies using transgenic mice support cardioprotection by α_{1a} rather than by α_{1b} (160). On the other hand, the β_2-adrenoceptor is reported to confer cardioprotection in ischemic preconditioning (209), whereas preischemic β_1-activation could be an alternative (193).

Indeed, reasons for such contradictions between the receptor blockade of ischemic preconditioning and pharmacological preconditioning with receptor agonists, or the inconsistency of positive or negative cardioprotection among the reports, are not fully understood. One reason for these differences may be due to the experimental models used; however, we should consider other reasons.

First, a feasible explanation is that there are multiple, parallel mechanisms induced by preconditioning ischemia, all of which can exert cardioprotection by themselves or in harmony. Accordingly, adenosine-dependent and α_1-adrenoceptor mechanisms might reflect this relationship (12, 214).

Second, pharmacological interventions do not necessarily mimic ischemic preconditioning accurately because of the half-life of mimetic agents; the majority of the agents might act for a longer period of time than the brief period of time required for preconditioning ischemia. Because the increased endogenous adenosine production induced by ischemic preconditioning confers cardioprotection in both preconditioning and reperfusion periods (95) and because adenosine-A_1 receptor activation around the onset of reperfusion also protects the myocardium (111), the preischemic administration of agents might still be effective beyond the sustained ischemic period.

Third, a critical time window for the involvement of the respective receptor activation is considered. For example, sustained transgenic activation of α_{1b}-adrenoceptor did not elicit cardioprotection (160), whereas temporal blockade during the preconditioning period protected the myocardium (68, 214). Also, β_1-adrenoceptor activation is reported to be beneficial during the preconditioning period but deleterious after reperfusion (193).

Finally, some reports do not support the contribution of adenosine in ischemic preconditioning-induced cardioprotection, because they failed to show that preconditioning-induced cardioprotection resulted in an increase in the intramyocardial level of adenosine. One possible reason for this failure might be due to how the level of adenosine was measured and the extremely short biological half-life of adenosine. We have also experienced this inconsistency when collecting samples without the prompt usage of a stop solution containing EDTA, adenosine deaminase inhibitors, and dipyridamole. Therefore, this may be due to the prompt intracellular uptake or ultrarapid degradation of adenosine under physiological conditions. Accordingly, this idea might be further supported by the observation that the loss of cardioprotection by the addition of exogenous adenosine was restored by extending its biological half-life by either a coadministration with dipyridamole to delay clearance through intracellular uptake (11) or a sustained targeting release using a liposomal envelope (201).

Further pharmacological analyses revealed the importance of other G protein-coupled receptor (GPCR) members, opioid receptors (22, 181), and bradykinin-B_2 receptors (52, 101) in pharmacological and ischemic preconditioning-induced cardioprotection in both the early (181) and late (22) phases of ischemic preconditioning. For example, the contribution of each opioid receptor (δ-, κ-, and μ-subtypes) has been reported in direct (107), remote, (144) or secondary protection of cardiac myocytes by acting on the central nervous system (106). However, the protection in the clinical setting still remains controversial (206, 219). As is summarized in Fig. 4, *top left*, various endogenous as well as exogenous stimulants cause their respective cardioprotective effects via the activation of unique or combined GPCR subtypes.

Downstream of GPCR: PKC, PKA cascades, and more. GPCRs couple to G proteins, consisting of a Gα- and a Gβγ-subunit, and the overall properties of each GPCR upon activation are generally defined by Gα-subtypes, such as G_s, G_i, and G_q. G_s and G_i positively and negatively modulate, respectively, cAMP production, whereas G_q activates phospholipase C and leads to PKC activation (Fig. 4).

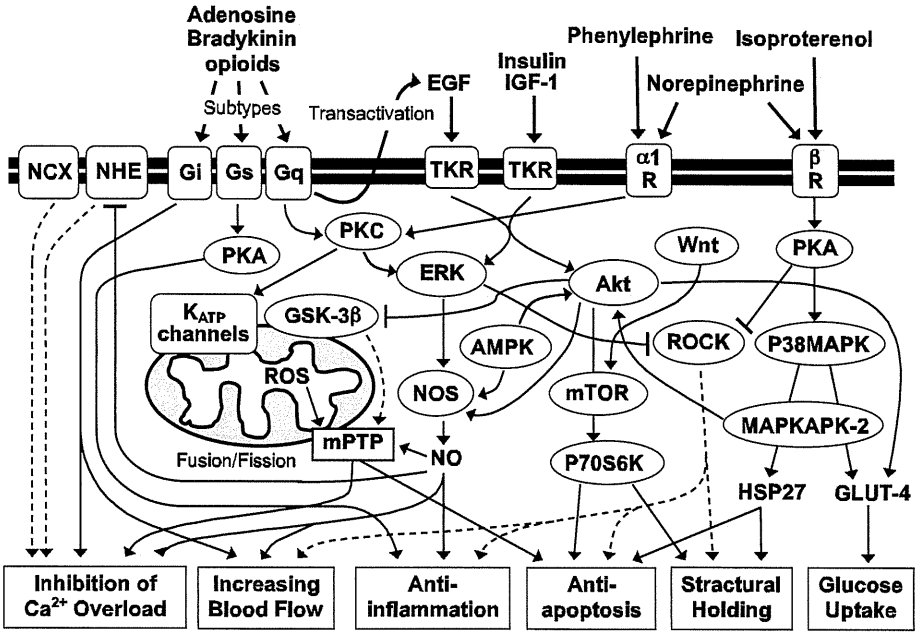

Fig. 4. Putative major cascades of cardioprotection and phenotypes of protection, afforded by preconditioning and postconditioning, either by brief ischemia(s) or by pharmacological agents. NCX, Na^+/Ca^{2+} exchanger; NHE, Na^+/H^+ exchanger; TKR, tyrosine kinase receptor, R, receptor; EGF, epidermal growth factor; IGF, insulin-like growth factor; mTOR, mammalian target of rapamycin; ROCK, Rho-associated protein kinase; K_{ATP}, ATP-sensitive K^+ channel; AMPK, 5′-AMP-activated kinase; NOS, nitric oxide (NO) synthase; MAPKAPK-2, MAPK-activated protein kinase 2; mPTP, mitochondrial permeability transition pore; HSP27, heat shock protein 27; GLUT-4, glucose transpoter 4. Dashed arrows indicate signal transduction through upstream inhibition.

Many reports have shown that ischemic preconditioning activates PKC (93, 237) and that PKC blockade abrogates infarct limitation induced by ischemic preconditioning (194, 237). In addition, repeated ischemic preconditioning instantly increases intramyocardial cAMP levels; moreover, either transient β-adrenoceptor stimulation (110) or intramyocardial pharmacological cAMP accumulation (167) mimics the cardioprotective behavior of preconditioning, and PKA inhibition significantly and substantially reduced the preconditioning-induced cardioprotection (167). Among PKC subtypes, PKC-δ inhibition or PKC-ϵ activation have been reported to be relevant to preconditioning-induced cardioprotection (186) in human myocardium, whereas we have previously reported the importance of Ca^{2+}-dependent, classic PKC in animal models (236).

As a possible downstream effector, we have previously reported that PKC directly activates ecto-5′-nucleotidase, located on the cell membrane (92), suggesting that adenosine could benefit the myocardium as not only a trigger but also a mediator of ischemic preconditioning (94). This has been supported by reports from other groups (95, 196). Recent reports also revealed that adenosine is an endogenous bioactive substance with multiple cardiovascular effects, including a negative inotropic effect, a negative contractile effect, and promotion of coronary blood flow and anti-platelet activity (90), as well as inhibition of apoptosis (158) and enhancement of autophagy (233). However, the role of elevated intramyocardial cAMP levels and PKA activation in cardioprotection of ischemic preconditioning has been reported (110), but they were both shown to be independent of PKC (117, 170, 176). Instead, mitochondrial ion channel (176) or p38 MAPK activation (170) was reported as a putative downstream mechanism in vivo. The reason for transient activation of p38 MAPK by PKA can be explained by PKA phosphorylation of the catalytic site of protein tyrosine phosphatase and inhibition of the dephosphorylation of p38 MAPK, leading to physiological augmentation of p38 MAPK activity (178). We also reported that Rho kinase plays an important role downstream of PKA during sustained ischemia to confer cardioprotection (167). Other reports support the involvement of SOD induction (48).

Taken together, while adenosine or α_{1b}-adrenoceptor stimulation could activate PKC (68) and while β_2-adrenoceptor or some unknown mechanism could activate PKA and cAMP response element-binding protein (119) following ischemic preconditioning, both mechanisms might independently but synergistically mediate preconditioning in response to various stimuli, including brief periods of ischemia (168). This might include a switch in second messenger signaling; cardioprotection that was induced by PKA activation through β_2-adrenoceptor stimulation was observed together with a switch of the second messenger from G_s to G_i (209). Also, α_{1b}-adrenoceptor stimulation resulted in PKC activation that was mediated by G_i, not G_q (68). Furthermore, a recent report (87) regarding heat-induced preconditioning intriguingly proposes p38 MAPK activation as a common cardioprotective mechanism in the PKC and PKA pathways.

p38 MAPK, ERK, and phosphatidylinositol 3-kinase/Akt cascades. The first report supporting the role of p38 MAPK activation during indexed ischemia in preconditioning-induced cardioprotection (221) was followed by opposing reports, in vivo (113) and in vitro (115), suggesting that p38 MAPK activation during prolonged ischemia could promote ischemic damage. In fact, continuous hypoxia causes biphasic activation of p38 MAPK in rat neonatal cardiomyocytes (115), with a transient peak within 30 min, followed by continuous activation after 4 h, leading to the hypothesis that p38 MAPK activation might have diverse effects; transient activation is protective, whereas continuous activation is harmful. We observed in vivo (171) that brief preconditioning ischemia causes transient but robust activation of p38 MAPK, followed by inactivation of p38 MAPK during sustained ischemia. The inhibition of p38 MAPK during the preconditioning period substantially blunted infarct limitation by ischemic preconditioning, implying a major role for p38 MAPK activation before

index ischemia in preconditioning-induced cardioprotection. However, Marber and colleagues (177) have shown in vitro a p38 MAPK subtype specificity in cardioprotection and that ischemic preconditioning reversed p38 MAPKα activation during index ischemia, whereas p38 MAPKβ was inhibited during index ischemia in the presence and absence of ischemic preconditioning. They have also shown that TGF-β-activated kinase-1-binding protein-1 might be important in this subtype-specific action of p38 MAPKα (205). While we also documented partial cardioprotection by nonspecific pharmacological p38 MAPK inhibition during index ischemia in the above study (171), the critical role of MAPKs during sustained ischemia in preconditioning-induced cardioprotection remains obscure (17).

As downstream effectors, p38 MAPK and phosphatidylinositol 3-kinase (PI3K) induce expression, membrane transportation, and activation of glucose transporter-4, which facilitates glucose uptake (191), partly regulated by 5′-AMP-activated kinase (138). Furthermore, MAPK-activated protein kinase-2 and HSP27 are also activated in the preconditioned myocardium at the onset of sustained ischemia (171). HSP27 binds to the z-bands of myofibrils and prevents ischemic myofilament degradation and the interaction of apoptotic protease-activating factor-1 with procaspase-9 by binding to cytochrome-*c* and reducing apoptotic changes (24). Interestingly, MAPK-activated protein kinase-2 also potentially activates Akt, another possible antagonist of apoptotic signals (157).

By contrast, the pharmacological and ischemic preconditioning-induced activation of ERK, another component of MAPKs, also plays an important role in cardioprotection. Initial findings showed that the inhibition of ERK during preconditioning and after reperfusion blunted the infarct limitation of ischemic preconditioning (196). Later reports indicated limited or enhanced MAPK contribution to cardioprotection during sustained ischemia (17) or after reperfusion (155), respectively, supporting the protective role of postischemic ERK activation in preconditioning-induced cardioprotection. Intriguingly, a counteracting effect of Rho-kinase activation at reperfusion is raised as a putative mechanism downstream of ERK (241). We have also observed this in vivo downstream of preischemic p38 MAPK activation (167). The cross talk between p38 MAPK and ERK in preconditioning-induced cardioprotection might be an important issue for further analysis.

PI3K and Akt, which are activated by ischemic preconditioning, are denoted as "reperfusion injury salvage kinase (RISK) pathways" (63), a set of signals together with ERK that confer cardioprotection against ischemia-reperfusion. They are also reported to induce nitric oxide (NO) production upon both ischemic preconditioning (211) and reperfusion (21); additionally, they are reported to protect the myocardium. We will discuss this later.

Finally, the cascades shown above are summarized in Fig. 4, *right*.

NO and cGMP pathways. NO is reported as a major factor that primarily provides cardioprotection (20). Unlike adenosine, NO can activate guanylate cyclase to use cGMP as a second messenger while exerting similar cardiovascular effects. The sources of NO can be both endogenous and exogenous. Although it still remains somewhat controversial (137), endogenous NO generated by either activated endothelial NO synthase (NOS) or upregulated inducible NOS can confer cardioprotection both immediately and long after the triggering signal, respectively (20). This supports the idea that NO works as both a signal mediator and an effector (90, 109), both immediately after ischemic insult and at later time points.

Recently, numerous reports revealed that the cardioprotective properties of NO are partly induced by vasodilation hemodynamic effects or anti-inflammatory effects (142), which are generally cGMP dependent (33) and similar to adenosine (168). However, they also include direct cGMP-independent effects: the inhibition of GSK-3β (30), which might cause the aforementioned cardioprotection as well as the inhibition of mitochondrial permeability transition pore (mPTP) (143) and the opening of the mitochondrial K_{ATP} channel, which are both dependent on (25) and are independent of (30) cGMP-mediated signaling. It is likely that the direct effects of NO largely target mitochondria. NO might also protect the myocardium by preventing mitochondrial fission (35, 141), opening mitochondrial K_{ATP} channel, and inhibiting mPTP to maintain energy metabolism against ischemic energy disturbances. We will discuss these issues in detail later.

While NO confers many aspects of cardioprotection as described above, the induction of NO synthesis colocalizes with the site of Ca^{2+} and ROS in action. NO could act as a double-edged sword when simultaneously exposed to excessive oxidative stress, resulting in both the uncoupling and generation of further oxidative/nitrosative stress (142).

K_{ATP} channels. The K_{ATP} channel, usually an octamer [4 inward rectifier K^+ channel (Kir) family and 4 sulfonylurea receptor (SUR) subunits] on the membrane modulated by Mg and ATP (190), was first identified by cardiovascular physiology studies as a relaxing and negative inotropic factor (234).

K_{ATP} channels, which are inward rectifiers (190), can raise a depolarization threshold and reduce the excitation of either vascular smooth muscle or cardiomyocytes, resulting in intracellular Ca^{2+} unloading and reduced metabolic demand (190, 234). However, Inoue et al. (75) also found ATP-sensitive inward rectifier activity on the inner mitochondrial membrane, suggesting the existence of "mitochondrial K_{ATP} channels" in contrast to "sarcolemmal K_{ATP} channels." Cardioprotection derived from both subtypes has been previously reported (172). The concept of the mitochondrial K_{ATP} channel as a final effector of cardioprotection involves the stabilization of the mitochondrial inner membrane and the prevention of membrane uncoupling (57), which provides similar benefits with the inhibition of mPTP due to preconditioning (32). For example, δ-opioid receptor signaling might also contribute to preconditioning with K_{ATP} channels as a putative downstream mechanism, but it is also reported to be involved in GSK-3β inhibition (53) or mitochondrial PTP-induced cardioprotection (32). Accordingly, pharmacological K_{ATP} opening prevents not only ischemic damages but also cardiac remodeling due to chronic nonischemic stimuli (169), suggesting that this may be a putative therapeutic strategy.

GSK-3β and mPTP. In search of the downstream cascades of PI3K, Tong et al. (210) reported on the involvement of GSK-3β inhibition in the cardioprotection of ischemic preconditioning. The emerging importance of this kinase, which is inactivated through phosphorylation by PI3K, is supported by its multiple roles as a critical downstream mediator of ischemic or pharmacological preconditioning that are induced by opioids (53) or mitochondrial K_{ATP} channel openers (32). This kinase

subsequently confers either triggered or immediate cardioprotection and serves as a downstream effector of the Wnt/Frizzled pathway-induced cardioprotection (16). These roles implicate this developmental signal in cardioprotection afforded by preconditioning. It has also been reported to target the mammalian target of rapamycin, one of the major common downstream effectors of the PI3K/Akt pathways (217).

However, mitochondrial protection against ischemia-reperfusion is necessary to ensure cellular respiration and aerobic ATP generation and to inhibit the release of cytotoxic agents such as ROS and proapoptotic factors (such as cytochrome-*c*) from mitochondria upon myocardial stress (57). There were two great breakthroughs in the understanding of mitochondrial protection: the discovery of the mitochondrial K_{ATP} activity as described above in *K_{ATP} channels* and the discovery of mPTP (56, 57).

The mitochondrial outer membrane contains a pore protein called the voltage-dependent anion channel (VDAC) that lets nonspecific small substances of less than ~5 kDa into the intermembrane space and cytosol, whereas the inner membrane is less permeable and may let only molecules such as H_2O, O_2, CO_2, or NH_3 go through. Therefore, the mechanism that induces mitochondrial release of larger molecules, such as cytochrome-*c* under stress, was not well understood. Originally, VDAC was considered to be a crucial component of this canal but was ruled out later because the intrinsic apoptotic pathway was also induced in VDAC knockout mice (13). Currently, Halestrap et al. (56) propose that mPTP is composed of adenine nucleotide translocase, mitochondrial phosphate carrier, and their regulator cyclophilin-D. Ca^{2+} overload (57) or ROS (175) is crucial to open the pore that enables small molecules to pass between the mitochondrial matrix and cytosol, allowing for an H^+ influx into mitochondria. This cancels the membrane potential across the mitochondrial membrane and results in mitochondrial swelling and subsequent apoptotic changes (66).

Cyclosporine A binds to cyclophilin D, located on the mitochondrial inner membrane, and inhibits mPTP opening by causing its dissociation from mPTP and thereby facilitating pore opening induced by Ca^{2+} and ROS (27, 57). Ischemic preconditioning is also reported to prevent, upon ischemia-reperfusion, the mPTP opening downstream of GSK-3β (84) or PKC-ϵ (15), possibly through the modulation of cyclophilin D (62). Finally, these models conform well to the idea that both necrotic (128) and apoptotic (32, 238) cell death occurs upon ischemia-reperfusion injury, and both are reduced by ischemic preconditioning (70).

Further investigation of the intersectional relationship between the RISK/survival and Wnt/developmental pathways, as well as mPTP (a putative contributing mechanism), in cardioprotection is necessary.

Ca^{2+} and free radicals. Importantly, it is widely recognized that both Ca^{2+} and ROS serve as signaling mediators under physiological conditions, while the dose, time period, and location are critical (43). It is well known that intracellular Ca^{2+} overload or induction of ROS causes cellular damage because of ischemia-reperfusion injury, especially when it is prolonged or intense. Moreover, as described above in *NO and cGMP pathways*, even a typically beneficial signal such as NO could cause deleterious effects when colocalized with excessive oxidative stress (142). However, short or transient exposure to them is reported to be beneficial because of their ability to trigger ischemic preconditioning (139, 198) and postconditioning (29). In preconditioning mechanisms, intracellular Ca^{2+} is required to activate classical PKC, an important component for triggering the preconditioning signal (139). Also, the Ca^{2+}-activated K^+ channel protects the myocardium when it is activated at the time of reperfusion (176, 185). Furthermore, Ca^{2+} is indispensable for myocardial twitching (142) and for the generation of ROS from mitochondria (43) within physiological range. On the other hand, ROS can reciprocally modulate intracellular Ca^{2+} homeostasis (43), and the transient increase in ROS through the increase in NO levels can trigger both early (24, 137) and late (198) phases of ischemic preconditioning. However, the role of ROS as a final effector of cardioprotection is rather controversial, especially in postconditioning, as discussed in the next section.

We finally summarized these mitochondria-oriented protective mechanisms in Fig. 4, *bottom left.*

Cardioprotection Afforded by Postconditioning

Postconditioning, defined as brief periods of ischemia alternating with brief periods of reflow applied at the onset of reperfusion following sustained ischemia (143), has recently been shown to have potential as a novel cardioprotective intervention against ischemia-reperfusion injury (197, 218). Ischemic postconditioning results in cardioprotection similar to preconditioning and provides a variety of crucial clues to cardioprotective mechanisms that can be directly applied in the clinic (28). In contrast to preconditioning, cardioprotection from postconditioning requires the instant sequence starting from triggers, through mediators and leading to effectors. The question as to whether cardioprotection from preconditioning and postconditioning use different mechanisms is currently under discussion (143), together with supportive (230) or negative (242) reports for additional cardioprotection from preconditioning beyond concomitant ischemic postconditioning.

Critical conditions for ischemia and reperfusion/reoxygenation in postconditioning. Because the prompt recovery of intracellular pH and reoxygenation upon reperfusion causes Ca^{2+} overload or excessive ROS generation and enhanced reperfusion injury, reduction of the levels of intracellular Ca^{2+} or ROS is one of the critical strategies for preventing reperfusion injuries. The initial successful attempts to reduce these levels were done using acidic (97) or staged (67) reperfusion, which can temper the promptness of pH recovery and reoxygenation upon reperfusion. On the other hand, recent studies have proposed that postconditioning can also elicit cardioprotection; however, it might instead induce the chances of repeated overshooting of intracellular Ca^{2+} and ROS levels at the time of reperfusion when preventive action has to take place. Accordingly, the latest reports have revealed that the benefits of postconditioning require the following conditions to be optimal: the duration of the index ischemia (118), the duration between the onset of reperfusion and the first brief ischemia, the duration and number of ischemias, and the duration of the interspersed reperfusion (143). First, postconditioning reduced the infarct size after index ischemia longer than 45 min in vivo, whereas it adversely impaired injury after index ischemia shorter than 30 min (118), possibly because the